


# Assembly of photoactive orange carotenoid protein from its domains unravels a carotenoid shuttle mechanism

Marcus Moldenhauer<sup>1</sup> · Nikolai N. Sluchanko<sup>2,3</sup> · David Buhrke<sup>1</sup> · Dmitry V. Zlenko<sup>3</sup> · Neslihan N. Tavraz<sup>1</sup> · Franz-Josef Schmitt<sup>1</sup> · Peter Hildebrandt<sup>1</sup> · Eugene G. Maksimov<sup>3</sup> · Thomas Friedrich<sup>1</sup> 

Received: 1 February 2017 / Accepted: 7 February 2017  
© Springer Science+Business Media Dordrecht 2017

**Abstract** The photoswitchable orange carotenoid protein (OCP) is indispensable for cyanobacterial photoprotection by quenching phycobilisome fluorescence upon photoconversion from the orange OCP<sup>O</sup> to the red OCP<sup>R</sup> form. Cyanobacterial genomes frequently harbor, besides genes for orange carotenoid proteins (OCPs), several genes encoding homologs of OCP's N- or C-terminal domains (NTD, CTD). Unlike the well-studied NTD homologs, called Red Carotenoid Proteins (RCPs), the role of CTD homologs remains elusive. We show how OCP can be reassembled from its functional domains. Expression of *Synechocystis* OCP-CTD in carotenoid-producing *Escherichia coli* yielded violet-colored proteins, which, upon mixing with the RCP-apoprotein, produced an orange-like photoswitchable form that further photoconverted into a species that quenches phycobilisome fluorescence and is

spectroscopically indistinguishable from RCP, thus demonstrating a unique carotenoid shuttle mechanism. Spontaneous carotenoid transfer also occurs between canthaxanthin-coordinating OCP-CTD and the OCP apoprotein resulting in formation of photoactive OCP. The OCP-CTD itself is a novel, dimeric carotenoid-binding protein, which can coordinate canthaxanthin and zeaxanthin, effectively quenches singlet oxygen and interacts with the Fluorescence Recovery Protein. These findings assign physiological roles to the multitude of CTD homologs in cyanobacteria and explain the evolutionary process of OCP formation.

**Keywords** Orange carotenoid protein · Cyanobacteria · Photoprotection · Photoactivity · Phycobilisome fluorescence quenching · Mass spectrometry · Analytical size-exclusion chromatography · Raman spectroscopy · UV–Vis spectroscopy · Carotenoid shuttle

Marcus Moldenhauer and Nikolai N. Sluchanko have contributed equally to this work.

**Electronic supplementary material** The online version of this article (doi:10.1007/s11120-017-0353-3) contains supplementary material, which is available to authorized users.

✉ Eugene G. Maksimov  
emaksimoff@yandex.ru

✉ Thomas Friedrich  
friedrich@chem.tu-berlin.de

<sup>1</sup> Institute of Chemistry PC 14, Technical University of Berlin, Straße des 17. Juni 135, 10623 Berlin, Germany

<sup>2</sup> A.N. Bach Institute of Biochemistry, Federal Research Center “Fundamentals of Biotechnology”, Russian Academy of Sciences, Moscow, Russian Federation 119071

<sup>3</sup> Department of Biophysics, Faculty of Biology, M.V. Lomonosov Moscow State University, Moscow, Russian Federation 119992

## Abbreviations

OCP <sup>O</sup>	Orange carotenoid protein—holoprotein, orange form
OCP <sup>R</sup>	Orange carotenoid protein—holoprotein, red form
RCP	Red carotenoid protein—holoprotein
Apo-RCP	N-terminal domain of <i>Synechocystis</i> OCP (amino acids 1–164)—apoprotein
COCP	C-terminal OCP-related carotenoid protein (C-terminal domain of <i>Synechocystis</i> OCP, amino acids 165–317)—holoprotein
Apo-COCP	C-terminal domain of <i>Synechocystis</i> OCP (amino acids 165–317)—apoprotein
<i>Synechocystis</i>	<i>Synechocystis</i> sp. PCC 6803
FRP	Fluorescence recovery protein
HCP	Helical carotenoid protein

StARD1	Human steroidogenic acute regulatory protein
ECN	Echinenone ( $\beta,\beta$ -Carotene-4-one)
CAN	Canthaxanthin ( $\beta,\beta$ -Carotene-4,4'-dione)
ZEA	Zeaxanthin ( $\beta,\beta$ -Carotene-4,4'-diol)
NTD	N-terminal domain
CTD	C-terminal domain
NPQ	Non-photochemical quenching
PBs	Phycobilisome
<i>E. coli</i>	<i>Escherichia coli</i>
SDS-PAGE	Sodium dodecyl sulfate polyacrylamide gel electrophoresis
LC-MS	Liquid chromatography-mass spectrometry
RR	Resonance Raman
Mw	Molecular weight
$R_H$	Hydrodynamic radius
$R_g$	Radius of gyration
ROS	Reactive oxygen species
SOSG	Singlet oxygen sensor green
$^1\text{O}_2$	Singlet oxygen

## Introduction

If man were to see Life as a giant construction site, a superficial look on the beautiful colors of the over 700 carotenoids in nature would recognize them as decoration work, and all but sophisticated inspection would disclose them as integral parts of its solar power plants, while at the same time forming the protective shield for its light-stricken engines. Along these lines, carotenoids are employed in light-harvesting photosynthesis as accessory pigments of photosystems and light-harvesting complexes, as well as in much simpler systems such as light-driven proton pumps from the microbial rhodopsin family, e.g., xanthorhodopsin (Luecke et al. 2008). At the same time, carotenoids perform protective roles against the harmful effects of solar irradiation either by dissipating excessively absorbed excitation energy or by their powerful antioxidative potential to scavenge radicals and reactive oxygen species (Schmitt et al. 2014). Photosynthesis involves the capture of light by the antenna complexes followed by excitation energy transfer to reaction centers, which convert light energy with high efficiency into chemical energy (Blankenship 2014; Mamedov et al. 2015; Mirkovic et al. 2016). A key requirement for photosynthetic organisms is the active control of the fragile balance between the beneficial and harmful effects of solar irradiation. While light harvesting at low light intensities is optimized by the employment of light-harvesting protein complexes, excessive excitation energy absorbed under high irradiance conditions must be dissipated by photoprotective mechanisms including the process of non-photochemical quenching (NPQ) (Demmig-Adams

and Adams 1996; Demmig-Adams et al. 2014; Niyogi and Truong 2013).

Cyanobacteria employ xanthophylls in a special manner due to the fact that their light-harvesting protein complexes, the phycobilisomes (PBs), are water-soluble. Cyanobacterial evolution developed special carotenoid-binding proteins which are directly photoswitchable and shuttle xanthophylls to the PBs when needed to enact quenching of PBs fluorescence, in order to shield the reaction centers from the harmful effects of excessively absorbed excitation energy (see Govindjee and Shevela 2011) for a perspective on cyanobacteria, as well as (Bryant 1994) and (Shevela et al. 2013) for overviews).

The 35 kDa photoactive orange carotenoid protein (OCP) plays a central role in cyanobacterial photoprotection. Upon illumination with blue light, OCP undergoes photo-transformation from the basic, orange form OCP<sup>O</sup> into the red signaling form OCP<sup>R</sup> (Gwizdala et al. 2011; Kirilovsky and Kerfeld 2012; Maksimov et al. 2015b, 2014), the latter quenching the fluorescence of phycobilisome (PBs) antennae, thus preventing excessive energy flow to the photosystems to enact non-photochemical quenching (NPQ). Besides acting in NPQ, OCP is also an efficient quencher of singlet oxygen,  $^1\text{O}_2$  (Sedoud et al. 2014). Termination of NPQ and re-establishment of full antennae capacity invoke the action of the 14 kDa Fluorescence Recovery Protein (FRP) (Boulay et al. 2010; Gwizdala et al. 2011, 2013; Maksimov et al. 2015b). However, the site where FRP binds to OCP is still controversial (Boulay et al. 2010; Sluchanko et al. 2017; Sutter et al. 2013).

The X-ray crystal structure of the orange form of OCP from native cyanobacteria is known since many years (Kerfeld et al. 2003; Wilson et al. 2010), whereas the red form has evaded structural characterization so far due to its lower thermodynamic stability. Very recent revolutionary progress in recombinant protein production using xanthophyll-producing *Escherichia coli* strains (de Carbon et al. 2015; Maksimov et al. 2016), allowing for flexible manipulations of the OCP sequence and the nature of bound carotenoids, has greatly simplified the expression of OCP proteins for functional and structural studies (Maksimov et al. 2016, 2017; Sluchanko et al. 2017; Thurotte et al. 2015; Gupta et al. 2015; Leverenz et al. 2015; Melnicki et al. 2016). OCP consists of two distinct structural domains, an N- and a C-terminal domain (NTD, CTD), connected via a linker that plays an important role in holding NTD and CTD together upon OCP photoactivation and domain separation (Gupta et al. 2015; Leverenz et al. 2014). A recent survey of 255 cyanobacterial genomes revealed that 87 thereof contain at least one homolog of the NTD, from which the majority (83) also contain a homolog of the CTD (Melnicki et al. 2016). This suggests that combinatorial heteromeric

assemblies of isolated NTDs and CTDs could substantially expand the versatility of sensor/effector activities based on OCP's modular architecture (López-Igual et al. 2016; Melnicki et al. 2016). However, while the role of the NTD, also known as Red Carotenoid Protein (RCP) (Leverenz et al. 2015), and its homologs from the helical carotenoid protein (HCP) superfamily is well established as phycobilisome fluorescence and singlet oxygen quenching (López-Igual et al. 2016), the role of the CTD and its multitude of homologs in numerous species is elusive.

## Materials and methods

### cDNA constructs and cloning

The cDNA constructs for expression of OCP and FRP from *Synechocystis* have been described (Maksimov et al. 2016; Sluchanko et al. 2017). The cDNA of *Synechocystis* OCP-CTD (termed COCP herein) was subcloned into the pQE81L vector resulting in the amino acid sequence (*Synechocystis* OCP amino acid numbering): MRGSH-HHHHTDPAT-A(165)...R(317). For the N-terminal domain of OCP (=RCP), a Stop codon was inserted at amino acid position 165. The Trp-288-Ala mutation (*Synechocystis* OCP numbering) was introduced by mutagenesis, and all cDNAs were verified by sequencing.

### Protein expression and purification

Carotenoid-binding proteins were expressed in carotenoid-producing NEBturbo *E. coli* cells (New England Biolabs, Germany) employing the pACCAR25ΔcrtXZcrtO plasmid for synthesis of ECN/CAN or the pACCAR25ΔcrtX plasmid for ZEA biosynthesis (Misawa et al. 1995), as described previously, and protein expression and purification also followed published procedures (Maksimov et al. 2016). Purified proteins were stored at  $-80^{\circ}\text{C}$  in PBS buffer (contents in mM: 137 NaCl, 2.7 KCl, 10  $\text{Na}_2\text{HPO}_4$ , 1.8  $\text{KH}_2\text{PO}_4$ , pH 7.4) until use. Phycobilisome purification and concentration measurement was conducted according to the procedures described in Sluchanko et al. (2017).

### Absorption measurements

Absorption spectra were recorded using a Cary 1E Varian spectrophotometer (Agilent Technologies, USA) at  $22^{\circ}\text{C}$ . To induce  $\text{OCP}^{\text{O}} \rightarrow \text{OCP}^{\text{R}}$  photoconversion, a 900 mW blue

LED (M455L3; Thorlabs, USA) with 455 nm maximum emission was used.

### Determination of carotenoid content

The carotenoid content of the carotenoid-binding proteins was determined after carotenoid extraction from purified proteins with acetone as described earlier (Choi et al. 2005). The carotenoids were extracted by adding 500  $\mu\text{L}$  acetone to 100  $\mu\text{L}$  of concentrated protein samples. The precipitated proteins were separated from the yellow supernatant by centrifugation at maximum speed for 3 min. Liquid chromatography/mass spectrometry (LC-MS) analysis was carried out on 20  $\mu\text{L}$  samples of extracted carotenoids using a LTQ Orbitrap XL (Thermo Fischer Scientific, USA) with a APCI source coupled to a HPLC 1200 system (Agilent Technologies, USA). The HPLC was performed on a TSK-GEL ODS-80Ts (Tosoh GmbH, Germany) C18 reverse-phase columns (150×3.2 mm and 150×4.6 mm) with eluent 1 (MeOH/Water 95:5; v:v) and eluent 2 (MeOH/THF 7:3, v:v) by using the following elution gradient: 0–5 min eluent 1 hold 100%, 5–10 min eluent 1 from 100 to 0% and eluent 2 from 0 to 100%, 10–18 min eluent 2 hold 100%, 18–23 min eluent 1 hold 100%, and a flow rate of 1 mL/min. The Agilent UV detector was set at 470 nm. Peak identification was based on mass spectrometry using the xcalibur program [Thermo Fisher Scientific;  $\beta$ -carotene 535 m/z, echinenone 550 m/z, canthaxanthin (564 m/z)]. Relative quantification (% of total carotenoids) was based on the response ratio of pigments measured at 470 nm and at  $\lambda_{\text{max}}$ , and extinction coefficients as published in Britton (1995).

### Analytical size-exclusion chromatography (SEC)

The oligomeric status of COCP, Apo-COCP, RCP, Apo-RCP and interaction of COCP or RCP with FRP were studied by analytical SEC as published before (Sluchanko et al. 2017). One hundred  $\mu\text{L}$  samples with varying protein concentrations were pre-incubated for 1 h at  $22^{\circ}\text{C}$  and analyzed using a Superdex 200 Increase 10/300 column (GE Healthcare, USA) equilibrated with a 20 mM Tris-HCl buffer, pH 7.55, containing 150 mM NaCl, 0.1 mM EDTA, 3% glycerol, and 3 mM  $\beta$ -mercaptoethanol, at a flow rate of 1.2 mL/min, while monitoring absorbance at 280 nm (Apo-COCP) or 540 nm (COCP). The column was calibrated by protein standards as described earlier (Maksimov et al. 2016; Sluchanko et al. 2017). To study COCP/FRP interaction, the individual proteins or their mixtures were pre-incubated for 1 h at  $22^{\circ}\text{C}$  and subjected to analytical SEC or non-denaturing gel electrophoresis, as described (Sluchanko et al. 2017). The fraction content of the tentative COCP/FRP complex separated by SEC was also analyzed

by SDS–PAGE. The same procedure was applied to study the oligomeric status of RCP and Apo-RCP, and its interaction with FRP.

### Resonance Raman (RR) spectroscopy

Spectra were recorded at  $-140^{\circ}\text{C}$  (Linkam cryostat, Resultec, Germany) using a Fourier Transform Raman spectrometer RFS-100/S (Bruker, Germany) equipped with a 1064 nm cw NdYAG laser (Compass 1064-1500N, Coherent LaserSystems, Germany) as described (Velazquez Escobar et al. 2013). Although 1064 nm excitation is not in resonance with chromophore absorption, the chromophore signals are  $\sim 1000$  fold enhanced over the protein bands justifying use of the term ‘resonance Raman’ (RR) spectroscopy for our pre-resonant conditions. For each RR spectrum, 2000 single scans were averaged. All samples were prepared at an  $\text{OD}_{280\text{nm}}$  of  $\sim 20$  in 50 mM Tris–HCl buffer, pH 7.8, containing 300 mM NaCl. For photoconversion, a 900 mW LED (M455L3; Thorlabs, USA) was used. Residual  $\text{OCP}^{\text{O}}$  contributions were subtracted from the  $\text{OCP}^{\text{R}}$  spectrum using an iterative method. A baseline correction was carried out using OPUS software (Bruker, Germany). Room-temperature Resonance Raman experiments were performed as described (Maksimov et al. 2015c).

### ROS quenching

In order to determine  $^1\text{O}_2$  quenching activity, we produced  $^1\text{O}_2$  by illumination of buffer solutions (20 mM Tris, 100 mM NaCl, 0.1 mM EDTA) containing either tetra- and pentakis(cholinile) aluminum phthalocyanines (AIPCs, 4  $\mu\text{M}$ ) (Maksimov et al. 2015a) or Rose Bengal (1  $\mu\text{M}$ ) in PBS buffer and used the fluorescence of Singlet Oxygen Sensor Green (SOSG, Molecular Probes, Germany) as indicator for  $^1\text{O}_2$  generation. Addition of carotenoid proteins caused a profound reduction of  $^1\text{O}_2$  yield compared to protein-free solutions. Importantly, protein samples were dialyzed before ROS quenching experiments to remove sodium azide, normally used for storage.

### PBs fluorescence quenching

The fluorescence measurements were performed using a FluoroMax-4 spectrofluorimeter (Horiba Jobin Yvon, Japan-France). Samples were diluted with 0.8 M phosphate buffer, pH 7.0. PBs concentration was constant in all experiments and equal to 50 nM. All experiments were conducted at  $20^{\circ}\text{C}$  and constant stirring at 600 rpm. PBs fluorescence was excited by 635 nm laser and the time-courses of fluorescence intensity at 680 nm were recorded with 0.1 s time resolution. Injection of 500 nM RCP caused reduction of PBs fluorescence in the dark, which

was considered as maximal possible effect for the current quencher-to-PBs ratio and thus used for normalization. The same concentration of Apo-RCP had no effect on PBs fluorescence. 500 nM of COCP caused a slight increase of PBs fluorescence in the dark. Addition of the mixture of Apo-RCP and COCP (in 5:1 ratio as shown in Fig. 4a, resulting final COCP concentration of 500 nM) containing orange-like heterodimers did not change PBs fluorescence until the sample was illuminated by actinic light (Blue LED M455 L3; Thorlabs, USA), which caused quenching of PBs fluorescence.

### Circular dichroism (CD) measurements

CD spectra in the UV (185–260 nm) and Vis (300–650 nm) range were recorded with a J-1100 CD spectrometer (Jasco GmbH, Germany). In addition to CD spectra in the far UV range, we also measured CD spectra within the visible range of wavelengths, where light absorption due to the strong  $\text{S}_0\text{--}\text{S}_2$  transition of carotenoids takes place. Since the embedment of otherwise rather symmetrical and therefore achiral chromophore-like carotenoids into an asymmetrical protein matrix leads to induced circular dichroism within the range of the visible absorption spectrum, these spectra give further insight into carotenoid–protein interactions (Chabera et al. 2011). For UV-CD spectra, protein samples of  $\sim 10$   $\mu\text{M}$  concentration were prepared in 30 mM sodium phosphate buffer, pH 7.4. For Vis-CD spectra, the samples were  $\sim 50$   $\mu\text{M}$ . For each sample, three UV- and Vis-CD spectra were recorded at room temperature and averages were calculated. The Vis-CD spectrum of the photo-switched  $\text{OCP}^{\text{R}}$  sample was recorded at  $4^{\circ}\text{C}$  after photoconversion by 5-min illumination with a blue 900 mW LED (M455L3; Thorlabs, USA). The Vis-CD spectra were normalized to the OD value at the maximum of the visible absorption spectrum, which implicitly assumes that the extinction coefficients of the different protein species are similar.

### Molecular dynamics simulations

The initial state for molecular dynamics (MD) simulations was composed from two C-terminal domains (amino acids 172–311) of OCP from *Synechocystis* sp. PCC 6803 [PDB 3MG1, (Wilson et al. 2010)]. Two carotenoid molecules from 3MG1 were superimposed in an anti-collinear manner and aligned atom-by-atom. The final structure was composed of two keto ring-containing halves of carotenoid molecules linked to each other and two corresponding OCP-CTDs. The GROMACS 5.0.6 software package was used for MD simulations (Abraham et al. 2015). The molecular topology of CAN was developed using standard OPLS atom types with a conjugated diene types for the

chain. TIP3P was used for water simulation. The molecular scene was orthorhombic with periodic boundary conditions and an interplane distance of 10 nm. The NaCl concentration was 150 mM. The stochastic dynamics integrator was used in NPT ensemble (Nose–Hoover for temperature- and Parrinello–Rahman for pressure-coupling) with integration steps of 2 fs and constraints (LINKS) on hydrogen atoms. After 600 ns of simulation, the structure was stabilized. Simulations were made using the supercomputer SKIF “LOMONOSOV” of the Supercomputer Center of Lomonosov Moscow State University.

## Results and discussion

### Structural organization of a unique carotenoid-binding protein, COCP

Upon expression of the 18 kDa OCP-CTD from *Synechocystis* sp. PCC 6803 in *E. coli* strains producing echinenone (ECN) and canthaxanthin (CAN), an unprecedented, deeply violet-colored protein was obtained (Fig. 1a, inset). The protein was not photoactive, since no changes in the absorption spectrum in the visible region were observed upon strong blue-light illumination (Supplementary Figure S1A). Since it represents a novel carotenoid-binding entity distinct from other known OCP-related proteins, we named this protein C-terminal OCP-related Carotenoid Protein, COCP, to discriminate it from its N-terminal counterpart, RCP.

According to far UV-CD spectroscopy data (Supplementary Figure S2), the secondary structure of purified COCP corresponded perfectly to the CTD folding from the latest OCP crystal structure (PDB 4XB5; residues 165–317), which contains 25 residues in  $\alpha$ -helices (16.4%) and 52 residues in  $\beta$ -strands (34.2%). In line with this,

deconvolution of the UV-CD spectrum of the COCP protein using the CDSSTR algorithm of the DichroWeb server (Whitmore and Wallace 2004) yielded 15%  $\alpha$ -helices and 32%  $\beta$ -strands (NRMSD=0.027), suggesting an unperturbed conformation. We found remarkable similarity between the secondary structure content of COCP and the unrelated  $\alpha/\beta$ -folded human steroidogenic acute regulatory protein (StARD1) (Sluchanko et al. 2016) (Supplementary Figure S2), whose close homolog, StARD3, was found to bind the carotenoid lutein in human retina (Li et al. 2011). On SDS–PAGE, the violet COCP (and the colorless apo-protein thereof, Apo-COCP) migrated as a single band of ~18 kDa (Fig. 1a,b insets). However, in analytical size-exclusion chromatography (SEC), COCP and Apo-COCP eluted significantly earlier than expected for their monomers, suggesting that a higher-order oligomeric form is present (Fig. 1a,b). For the violet COCP, molecular weight estimation based on column calibration resulted in a value of 38 kDa ideally corresponding to COCP dimers, with hydrodynamic radius  $R_H = 2.80$  nm (i.e., gyration radius  $R_g = 2.17$  nm for a near-spherical particle), and these dimers were stable even upon manifold sample dilution (Fig. 1a,c). In contrast, we observed strong concentration-dependent dissociation in the case of Apo-COCP (Fig. 1b,c), from near-dimeric (34 kDa) at higher, to almost completely monomeric forms (~20 kDa,  $R_H = 1.94$  nm) at lowest protein concentrations (Fig. 1a,c). Such a dynamic behavior of Apo-COCP and the stability of the violet COCP holo-protein unequivocally indicate that the carotenoid plays a significant structural role in stabilizing the assembly of the COCP homodimer.

In striking contrast, irrespective of the presence of a carotenoid, the second known OCP module, RCP (the 19.4 kDa NTD of OCP), was monomeric with an apparent molecular mass of 20.1 kDa, almost independent of protein concentration (Supplementary Figure S3). The

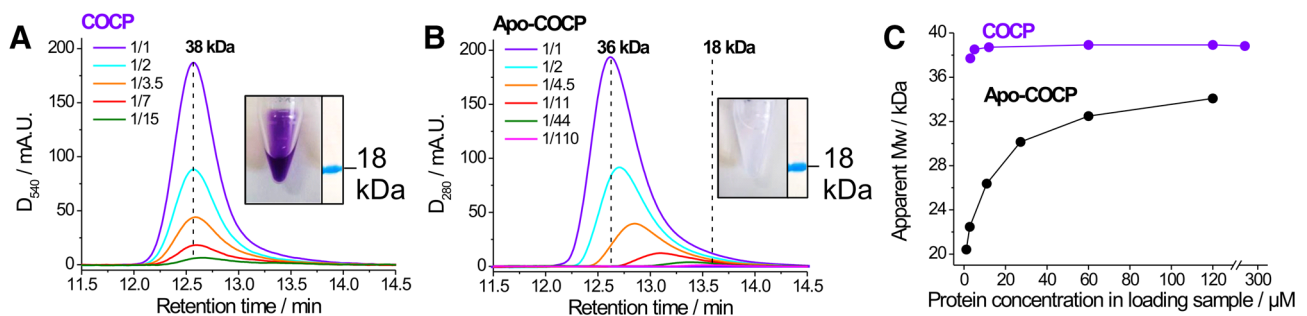


**Fig. 1** Oligomeric status of COCP and Apo-COCP determined by analytical SEC. **a** SEC elution profiles of COCP (detection: 540 nm) and **b** Apo-COCP (detection: 280 nm) at increasing dilutions as indicated (initial protein concentrations: COCP: 3.4 mg/mL; Apo-COCP: 2.1 mg/mL). *Insets* in (a,b) show solutions of the respective purified proteins and Coomassie brilliant blue-stained bands on SDS-

electrophoregrams with molecular weight (Mw) marker indicated. **c** Dependence of the apparent Mw on protein concentration for samples from **a** and **b** estimated for COCP and Apo-COCP based on a column calibration with protein standards of known Mw. See “Materials and methods” and (Sluchanko et al. 2017) for further details

strong concentration dependence of Apo-COCP observed here is remarkably similar to the previously reported concentration-dependent behavior of an OCP<sup>R</sup> analogue, the purple OCP<sup>W288A</sup> mutant protein (Maksimov et al. 2016). This distinct property of the OCP-CTD explains the pronounced propensity of the active quenching OCP forms to self-association and may be relevant for the photoprotection mechanism.

## Spectroscopic characterization of COCP

The homodimeric arrangement, having nearly half of the carotenoid-binding cavity in each CTD, suggests that one, most likely symmetric carotenoid molecule is attached in an equivalent fashion to two identical COCP monomers. Surprisingly, this was confirmed by liquid chromatography/mass spectrometry (LC-MS) data showing that COCP obtained from *E. coli* strains producing both ECN and CAN

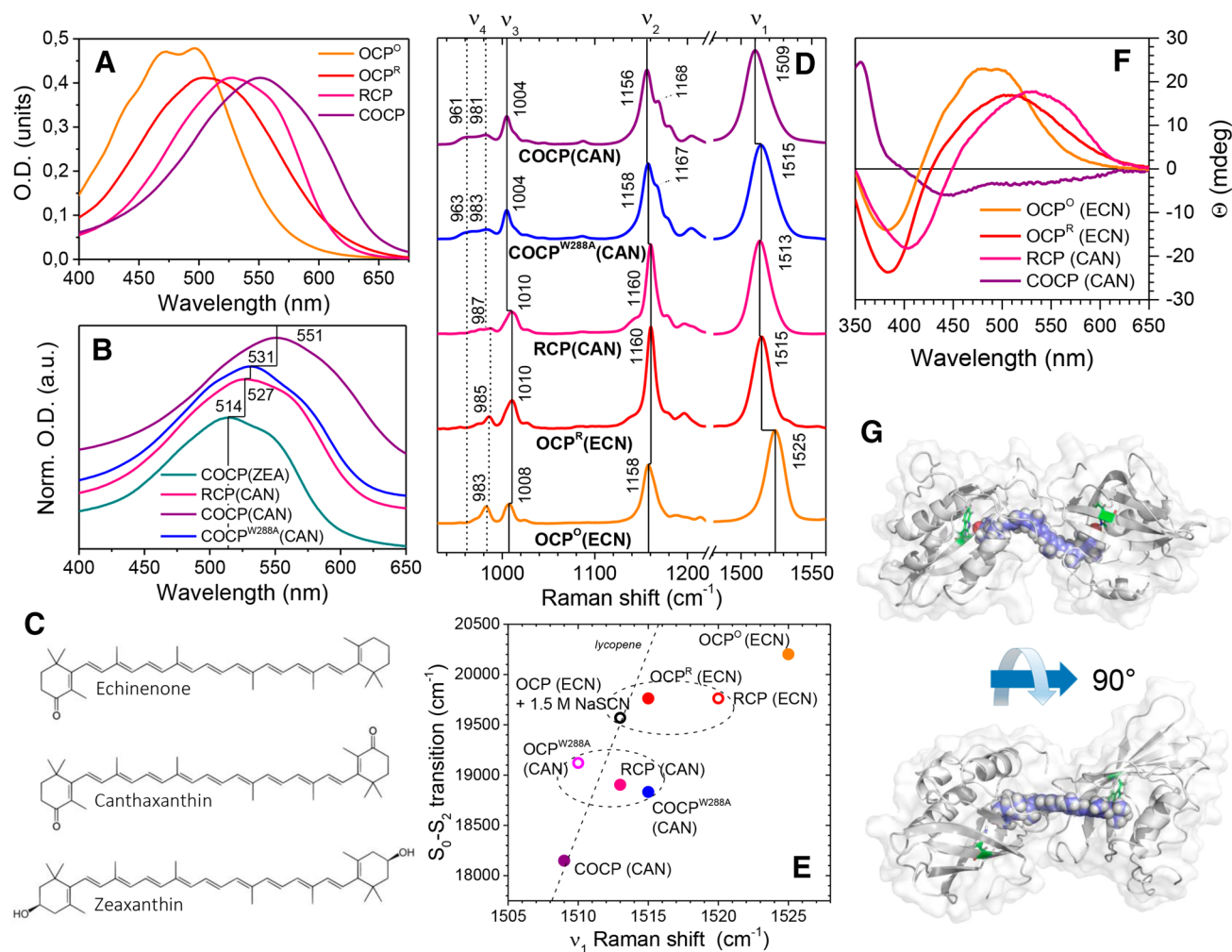


**Fig. 2** Spectroscopic properties of COCP and other OCP-related proteins. **a** Visible absorption spectra of COCP, RCP, and OCP in the orange and red state (OCP<sup>O</sup> and OCP<sup>R</sup>, respectively). For carotenoid content analysis, see Supplementary Figure S4. **b** Absorption spectra of COCP(CAN), COCP(ZEA), COCP<sup>W288A</sup>(CAN) and RCP(CAN). Spectra were shifted along the y-axis for better presentation. **c** Chemical structures of echinenone (ECN), canthaxanthin (CAN), and zeaxanthin (ZEA). **d** Pre-resonance Raman spectra of the orange and red OCP forms and its carotenoid-binding domains. Numbers above the lines indicate the positions of  $\nu_1$ - $\nu_4$  bands. **e** Correlation between the position of the  $S_0 \rightarrow S_2$  electronic transition and the  $\nu_1$  band frequency for different OCP forms. Open circles indicate parameters taken from the literature (Leverenz et al. 2014; Maksimov et al.

2016). The dashed line indicates the dependency of spectral characteristics of lycopene in different solvents (Kish et al. 2015). Dashed ellipses encompass various OCP-related proteins coordinating either ECN or CAN as cofactor indicating that the protein environment critically determines the position of the  $\nu_1$  Raman band, while the  $S_0 \rightarrow S_2$  transition energy is about the same. **f** Vis-CD spectra of the orange and red OCP forms and its individual carotenoid-binding domains. **g** Results of a molecular dynamics simulation experiment demonstrating the structure of the COCP homodimer composed of two OCP-CTD subunits [initial coordinates from PDB 3MG1 (Wilson et al. 2010)] coordinating one CAN molecule via H-bonds from Trp-288 in each subunit to the 4-(4')-keto groups at the terminal  $\beta$ -rings. For further explanation, see text and “Materials and methods”

(Fig. 2c) contains 95% of the symmetric CAN and only 5% ECN, in strong contrast to OCP, which mainly coordinates the asymmetric ECN under identical expression conditions (see Supplementary Information and Supplementary Figure S4).

Therefore, most probably, each monomer within the COCP homodimer coordinates one of the two 4-keto groups of the terminal  $\beta$ -rings of a single CAN molecule by the specific H-bond pattern observed in the crystal structures of OCP<sup>O</sup>. As a result, COCP(CAN) exhibits a unique absorbance spectrum, which is broad and without vibronic substructure (Fig. 2a). With a maximum at 551 nm, it is the most red-shifted from all OCP-like proteins reported to date, and even more red-shifted than the ones of RCP and of the purple OCP<sup>W288A</sup> mutant described previously (Sluchanko et al. 2017).

Interestingly, by utilizing *E. coli* strains tailored to synthesize the symmetric carotenoid zeaxanthin (ZEA), we again obtained colored COCP protein with a characteristic absorption spectrum (Supplementary Figure S1B), further supporting the general ability of the novel carotenoid-binding protein, COCP, to accommodate carotenoids with symmetrical  $\beta$ -ring structures. Of note, expression of a mutant COCP<sup>W288A</sup> carrying a substitution of the critical Trp residue involved in H-bonding with the 4-keto group of the xanthophyll (Maksimov et al. 2016; Sluchanko et al. 2017) in an ECN/CAN-producing *E. coli* strain again yielded a CAN-coordinating protein (Supplementary Figure S4), but with a less red-shifted absorption spectrum compared to COCP, very similar to the spectrum of RCP (Fig. 2b).

To get deeper insight into the chromophore structure, we scrutinized COCP by Raman (RR) and visible circular dichroism (Vis-CD) spectroscopy. RR spectra of COCP(CAN) and COCP<sup>W288A</sup>(CAN) were recorded and compared to the ones of other OCP variants characterized previously (Kish et al. 2015; Leverenz et al. 2014; Maksimov et al. 2016). In accordance with the established band assignment for carotenoids (Schlücker et al. 2003), the  $\nu_1$  band positions of COCP (1509 cm<sup>-1</sup>) and COCP<sup>W288A</sup> (1515 cm<sup>-1</sup>) conform with the well-known correlation between the  $\nu_1$  band position (for OCP<sup>O</sup>: 1525 cm<sup>-1</sup>; for RCP: 1513 cm<sup>-1</sup>) (Fig. 2d) and the spectral position of the chromophore's S<sub>0</sub>-S<sub>2</sub> transition inferred from the maximum of the absorption spectrum (Kish et al. 2015; Mendes-Pinto et al. 2013), and notably places the  $\nu_1$  band COCP on a correlation line determined for the linear C<sub>40</sub> carotenoid lycopene in solvents of different polarizability (Kish et al. 2015). Recent theoretical studies show that this correlation can be rationalized for different carotenoid-binding proteins by a combination of two effects: (i) the rotation of the  $\beta$ -ionone rings with respect to the conjugated system (Mori 2016) and (ii) the local electric field in the chromophore-binding pocket (Gamiz-Hernandez et al. 2015). As

discussed above, the preference of COCP for CAN over ECN points to the importance of H-bonding between the ketolated  $\beta$ -rings and Trp288/Tyr201 of COCP. Therefore, the effect of the W288A mutation (partly) disturbing this H-bonding pattern and inducing the correlated shifts between 1509 cm<sup>-1</sup> and 1515 cm<sup>-1</sup> band positions in RR spectra (Fig. 2d) and the profound (20 nm) blue-shift in the absorbance spectra (Fig. 2b) supports a structural model for COCP, in which a homodimer of two COCP subunits coordinates one CAN chromophore (Fig. 2g).

Compared to OCP<sup>O</sup> and RCP, the  $\nu_1$  bands of COCP and COCP<sup>W288A</sup> are significantly broader, indicating a larger structural flexibility of the carotenoid in these proteins. The  $\nu_2$  bands of COCP and COCP<sup>W288A</sup> are also broadened and exhibit significant splitting into two lines with another elevated shoulder on their high-energy flanges, suggesting a mixture of chromophore configurations. Significant differences can also be discriminated at the  $\nu_3$  band (composed of CH<sub>3</sub>-rocking vibrations) with a rather sharp peak at 1005 cm<sup>-1</sup> and a smaller at 1013 cm<sup>-1</sup>. Also, the low-energy flanges of the  $\nu_4$  band of COCP and the COCP<sup>W288A</sup> mutant are elevated, a unique feature that has not been previously observed in other OCP proteins. Since the  $\nu_4$  band comprises contributions from C-H hydrogen-out-of-plane (HOOP) modes at the polyene chain, which are not or only little Raman-active if the chromophore adopts a relaxed, planar structure as in RCP (Leverenz et al. 2014, 2015), the elevated Raman bands of the  $\nu_4$  region suggest a certain species with distorted or squeezed configuration of the carotenoid in COCP and COCP<sup>W288A</sup>, which is different from the one in OCP<sup>O</sup>, the latter showing the highest  $\nu_4$  band at 983 cm<sup>-1</sup>, but no Raman signals at the band's low-energy flange (960 cm<sup>-1</sup>).

To understand the possible chirality of the carotenoid environment created by its embedding into an asymmetric protein matrix, we recorded Vis-CD spectra of COCP and other OCP variants (Fig. 2f). The investigated CAN-constructs of RCP and COCP have lower ellipticities in the range of the visible absorption spectrum than all the ECN-containing variants of full-length OCP proteins, because (i) the symmetric CAN chromophore is inherently less chiral than ECN and (ii) the asymmetry of the protein environment is reduced, as suggested for the relation between OCP and RCP Vis-CD spectra (Chabera et al. 2011; King et al. 2014). In the RCP crystal structure (Leverenz et al. 2015), the chromophore is planar, with one  $\beta$ -ring rotated out-of-plane and the other coplanar with the polyene chain, which is most likely the reason for the low CD activity of RCP(CAN) (Chabera et al. 2011). The low Vis-CD intensity, the red-shifted absorption, and the low-energy  $\nu_1$  mode at 1509 cm<sup>-1</sup>, which correlates with the spectral features of lycopene (the C<sub>40</sub> carotenoid with the longest conjugated system possible), collectively indicate that in COCP both

$\beta$ -ionone rings are planar with respect to the conjugated system. This also coincides with crystal structures and calculations of various red-shifted carotenoid chromophores containing planar  $\beta$ -rings, e.g., of crustacyanin, which endows lobster carapace with its deep bluish-black color (Cianci et al. 2002; Gamiz-Hernandez et al. 2015). Furthermore, the unique HOOP band pattern of COCP indicates another type of non-planarity of the conjugated system compared to the lower intensity HOOP bands of the planar chromophore in RCP, which cannot be explained by a bending of the chromophore, because this would lead to the characteristic  $983\text{ cm}^{-1}$  band observed in OCP. Also, the deformation of the conjugated chain must be symmetric to be in accordance with the low-amplitude Vis-CD spectrum and the symmetric, homodimeric protein composition. Hence, we propose a symmetric squeezing and torsion of the conjugated chain of CAN in COCP, which is the only possible interpretation left (Fig. 2g). Interestingly, the novel HOOP motif of COCP is conserved in COCP<sup>W288A</sup>, whereas the  $\nu_1$  band of the latter is upshifted to  $1515\text{ cm}^{-1}$ , a position similar to RCP(CAN). These spectral features indicate that the structure of the conjugated chain and the overall protein configuration are approximately the same in COCP<sup>W288A</sup>, but the lack of stabilizing H-bonds at the  $\beta$ -rings leads to a symmetrical out-of-plane relaxation of the rings. The positions of the  $\nu_1$  band and the  $S_0$ - $S_2$  transition indicate that the rotational angle of both rings must be smaller than the rotation of the  $\beta_1$ -ring in RCP to bring about similar phenotypes in all spectroscopic features.

From all these spectroscopic and structural observations, we propose a structural model of COCP based on the crystal structure of the COCP coordinating CAN [PDB 3MG1,

(Wilson et al. 2010)]. After optimization by molecular dynamics simulations on a rather long 600 ns timescale (see “Materials and methods”), the model (Fig. 2g) represents a conformation consistent with our Vis-CD, RR, SEC, and secondary structure data, and its resultant radius of gyration ( $R_g$ ) value of 2.15 nm matches the one derived from analytical SEC (2.17 nm). The model shows the CAN chromophore with coplanar arrangement of the terminal  $\beta$ -rings relative to the polyene chain, with the preserved H-bonding of the keto groups with the Trp-288 residues in each COCP monomer.

### Functional properties of COCP

The FRP-binding site on OCP, albeit important for understanding their interaction during termination of PBs fluorescence quenching in the context of cyanobacterial photoprotection, still remains controversial (Boulay et al. 2010; Sluchanko et al. 2017; Sutter et al. 2013). To assess the possibility of a physical interaction between COCP and FRP, we employed analytical SEC (Fig. 3a) and native gel electrophoresis (Supplementary Figure S5). As shown earlier (Sluchanko et al. 2017) and above, both, FRP and COCP(CAN), eluted as 28.3 and 38 kDa dimeric proteins, respectively (Fig. 3a). COCP/FRP mixtures at an excess of FRP eluted as Peak I (Fig. 3a), which is substantially shifted relative to the COCP peak and corresponds to a species with an apparent Mw of 47.3 kDa. This implies the formation of a stable COCP/FRP complex at an apparent stoichiometry, that is, however, clearly distinct from a dimer/dimer assembly (theoretically ~66 kDa). Importantly, SDS-PAGE analysis confirmed the presence of both,

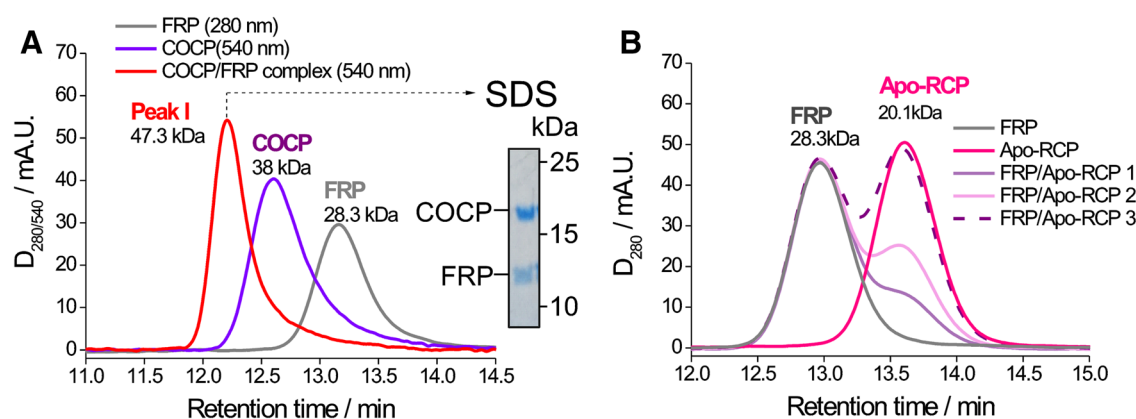


**Fig. 3** Interaction of functional modules of OCP, COCP and RCP with FRP analyzed by SEC. **a** Elution profiles of COCP (50  $\mu\text{M}$ ), FRP (18  $\mu\text{M}$ ), and a mixture of both (50  $\mu\text{M}$  COCP/70  $\mu\text{M}$  FRP) followed by absorbance at the indicated wavelengths. The inset shows a Coomassie brilliant blue-stained SDS-PAGE of the eluate from Peak I, with Mw markers and positions of COCP and FRP indicated. **b** Elution profile of FRP (26  $\mu\text{M}$ ), Apo-RCP (18  $\mu\text{M}$ ), or mixtures

of FRP (26  $\mu\text{M}$ ) with increasing amounts of Apo-RCP [4.3  $\mu\text{M}$  (1), 8.6  $\mu\text{M}$  (2), 18  $\mu\text{M}$  (3)], followed by absorbance at 280 nm. Note that profile 3 ideally coincides with the sum of individual FRP and Apo-RCP profiles, indicating no protein-protein interaction, and that the presence of carotenoids in COCP and RCP does not affect their ability to interact with FRP. See “Materials and methods” for details



COCP and FRP proteins, in Peak I (Fig. 3a, inset). Unfortunately, taking into account possible conformational changes upon complex formation, we cannot unambiguously delineate, whether the apparent Mw of 47.3 kDa corresponds to a stoichiometry of 2:1, 1:2, or a 1:1/2:2 mixture. Importantly, the COCP/FRP complex and its components could be separated by native gel electrophoresis (Supplementary Figure S5), which supports the conclusions from SEC data and confirms tight interaction of both, COCP and Apo-COCP, with FRP. In contrast, no evidence for such an interaction could be found for RCP/FRP mixtures analyzed by SEC. In contrast to COCP, and irrespective of the presence of carotenoid, RCP was present as a monomer at all concentrations tested (Fig. 3b and Supplementary Figure S3), and we failed to observe physical interaction between FRP and Apo-RCP taken in different concentrations (Fig. 3b). Although we cannot exclude that in the context of the full-length OCP, FRP may also contact the NTD, the CTD is individually capable of interacting tightly with FRP, suggesting that the main FRP-binding site is located on the OCP-CTD.

The ability of COCP to quench  $^1\text{O}_2$  was tested by illumination of common  $^1\text{O}_2$  sensitizers, either tetra- and pentakis(cholinile) aluminum phthalocyanines (AIPCs) (Maksimov et al. 2015a) or Rose Bengal (as used in previous  $^1\text{O}_2$  quenching assays (Kerfeld et al. 2003; Sedoud et al. 2014)), using Singlet Oxygen Sensor Green (SOSG) fluorescence to monitor  $^1\text{O}_2$  generation. Both, COCP and OCP caused a profound reduction of  $^1\text{O}_2$  yield (Supplementary Figure S6). Surprisingly, COCP appears to be an even better  $^1\text{O}_2$  quencher than OCP in the orange state in both assays. This ROS quenching ability of COCP suggests a photoprotective role of OCP-CTD homologs in vivo.

### Reassembly of a photoactive OCP from functional modules

Since the available OCP crystal structures suggest a specific interface between NTD and CTD involving the Arg-155/Glu-244 salt bridge, an extensively H-bonded interface between the N-terminal extension (residues 3–15 of *Synechocystis* OCP) of the NTD attaching several  $\beta$ -sheets on the CTD (Wilson et al. 2010), and a flexible loop of the CTD (residues 274–284) contacting the NTD from the opposite side, it seems probable that the two domains have an affinity to each other even when not physically linked. In order to test the possibility to reassemble a photoactive OCP protein from individual structural domains, we studied the absorption spectra of mixtures of (i) Apo-COCP and RCP, and (ii) COCP and Apo-RCP by mixing constant concentrations of the carotenoid-containing forms with increasing amounts of the apoprotein forms. We did not find any changes of RCP absorption upon addition of

Apo-COCP, in line with previous findings that partial proteolysis of OCP causes exclusive formation of RCP (Leverenz et al. 2014), suggesting that the carotenoid has higher affinity to the OCP-NTD (Leverenz et al. 2015). In contrast, addition of Apo-RCP to COCP caused dramatic changes of the absorption spectrum (Fig. 4a) indicating rearrangement of the chromophore's local environment. Surprisingly, the difference between the absorption spectra of COCP and mixtures with Apo-RCP is very similar to the light-minus-dark absorbance spectrum of full-length OCP (Maksimov et al. 2015c; Sluchanko et al. 2017; Wilson et al. 2008). Indeed, the vibronic substructure characteristic for OCP in the orange form appears upon addition of Apo-RCP to COCP, revealing peaks and shoulders at 498, 468, and 437 nm (Fig. 4a). However, even when Apo-RCP was present in large excess, the overall absorption changes between such a hybrid orange-like form and COCP were less than 50% compared to the spectral changes upon  $\text{OCP}^{\text{O}}$  and  $\text{OCP}^{\text{R}}$  photoconversion. This indicates a non-homogeneous distribution of the carotenoid, presumably, the presence of red (and violet) forms in addition to an orange-like protein. The limited efficiency of the process can be at least partially explained by the dimeric nature of COCP, requiring dimer dissociation for interaction with the NTD.

The formation of an orange-like form proves that the isolated NTD and CTD of OCP interact with each other tending to form a thermodynamically stable state. Next, we tested whether this state could be affected by actinic light, which triggers conversion of  $\text{OCP}^{\text{O}}$  to  $\text{OCP}^{\text{R}}$ , by measuring absorption changes at 550 nm upon illumination of the mixed sample by blue light. The obtained kinetics followed the time-course typical for the absorption change of the  $\text{OCP}^{\text{O}} \rightarrow \text{OCP}^{\text{R}}$  photoconversion and back-relaxation in the dark (Fig. 4c). Importantly, in the fully converted state, the absorption of the sample was not identical to the initial (violet) COCP, but remained significantly blue-shifted. In addition, after the illumination was turned off, the absorption at 550 nm decreased monoexponentially (Fig. 4c), but did not reach its initial value, indicating that parts of the sample had become trapped in the red state (Fig. 4b). This phenomenon can be explained by a light-induced separation of NTD and CTD, with the carotenoid shifted into the NTD, as it is thought to occur in full-length OCP (Gupta et al. 2015), but with the notable difference that there is no linker between the domains in our reconstructed system. Therefore, both domains might dissociate from each other upon photoconversion. As a result of this domain separation, Apo-COCP and RCP with CAN bound will be formed, which would fully explain the partial irreversibility of the spectral change observed upon such a light-triggered mechanism.

To additionally validate the hypothesis of a carotenoid shuttle mechanism between COCP and Apo-RCP, we

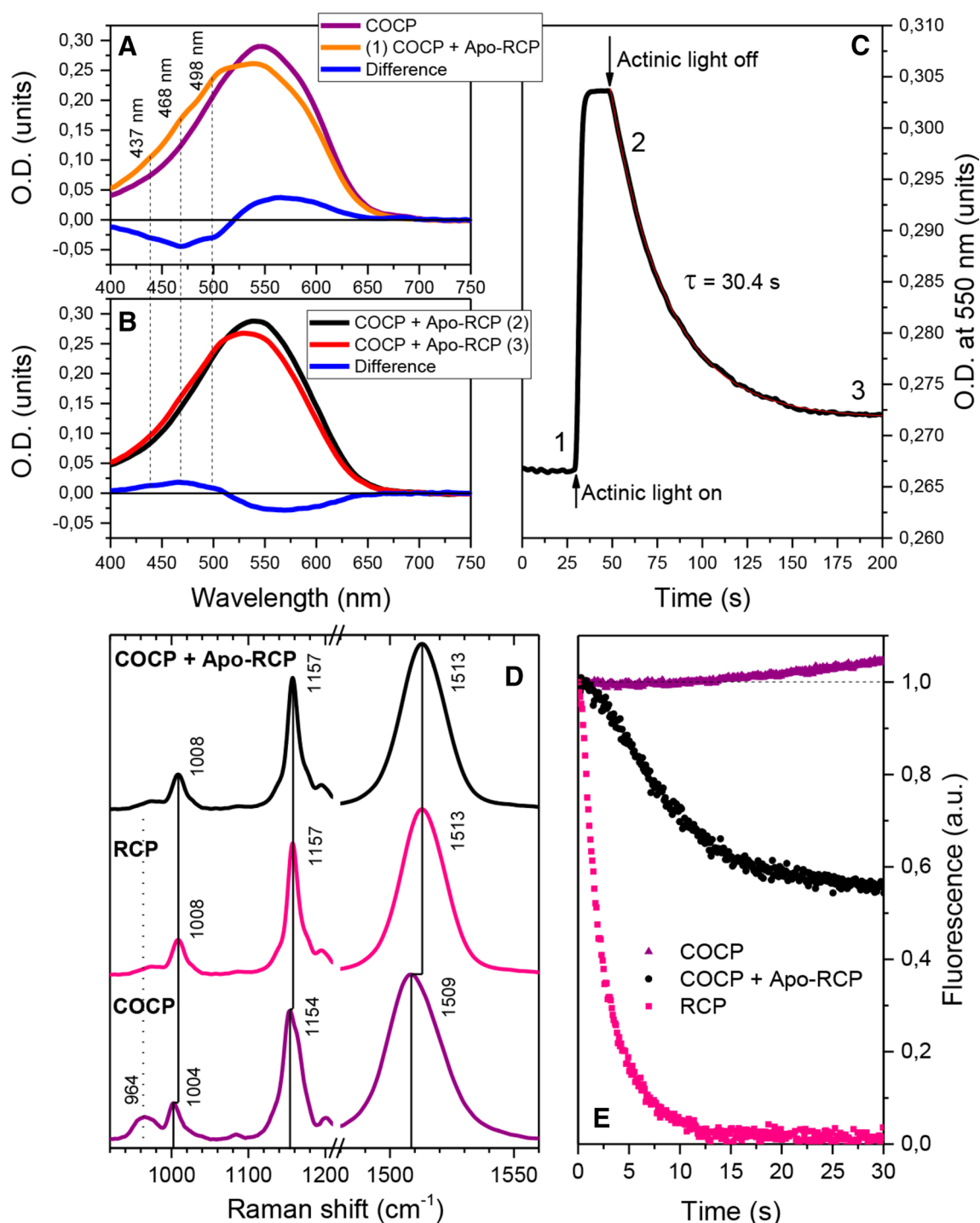


**Fig. 4** **a** Effect of Apo-RCP on the COCP absorption spectrum. Apo-RCP was added until the changes of absorption were saturated. **b** Illumination of the sample in the orange-like state causes a red shift (black curve), which is partially reversible (red curve), and a part of the sample returns into the orange-like state (indicated by the shape of the difference spectra in **a** and **b**). **c** Time-course of the optical density at 550 nm upon photoconversion (actinic light: 455 nm illumination)

and consequent relaxation of the sample. Numbers indicate at which moment on the time-course the numbered spectra in **a** and **b** were recorded. Absorption was measured at 25 °C and constant stirring. **d** Resonance Raman spectra of COCP, RCP and a mixture of COCP and Apo-RCP. **e** PBs fluorescence quenching in vitro induced by RCP (in the dark) and upon illumination of the sample containing a mixture of Apo-RCP and COCP

measured RR spectra of COCP, RCP, and a mixture of Apo-RCP with COCP obtained under conditions similar to the absorption experiments shown (Fig. 4a,b). Resonance Raman scattering was induced by focused 532 nm laser light, which rapidly converted any orange-like state into the red-like state. As shown in Fig. 4d, the RR spectrum of the COCP/Apo-RCP mixture is identical to the one of RCP, which supports our assumption regarding the domain separation upon photoconversion and the proposed carotenoid shuttle mechanism that ultimately results in formation of RCP. Also, we tested whether the photoactive protein formed from the COCP/Apo-RCP mixture is physiologically active and studied its effect on phycobilisome fluorescence quenching. With the PBs quenching effect of RCP as a reference (Fig. 4e), COCP alone did not quench PBs fluorescence. Rather, for an as yet unknown reason, a slight increase in PBs fluorescence was obtained. When kept in the dark, also the COCP/Apo-RCP mixture did not quench, but upon illumination with actinic light, a remarkable, sigmoidal decrease in PBs fluorescence was observed, substantiating our hypothesis that a quenching-competent OCP<sup>R</sup>-like state, and eventually RCP, is formed. Probably, the orange-like heterodimer could be stabilized by high phosphate concentration (0.8 M), which explains the lower quenching efficiency compared to the one of RCP.

Notably, the carotenoid shuttle mechanism demonstrated between COCP(CAN) and Apo-RCP also occurs in conjunction with the OCP apoprotein (Apo-OCP). As shown in Supplementary Figure S7A, immediately upon addition of Apo-OCP to COCP(CAN) in 1:1 molar ratio, the absorption spectrum undergoes a blue-shift, eventually

resulting in a species exhibiting spectral features of the OCP<sup>O</sup> state, as evident from the clear vibronic substructure of the resultant spectrum (compared to Fig. 2a). This newly formed OCP species is readily photoconvertible into the OCP<sup>R</sup> state upon illumination with actinic light from a blue LED (Supplementary Figure S7B). The photoconverted species slowly returns in the dark into the OCP<sup>O</sup> state, and photoswitching into the OCP<sup>R</sup> form can be repeated multiple times (data not shown). Of note, the photoswitchable OCP formed upon carotenoid transfer from COCP(CAN) harbors CAN as a chromophore instead of the ECN-bound OCP form, which is normally obtained under the same expression conditions in *E. coli* (Supplementary Figure S4). Thus, also the OCP apoprotein is able to break up the otherwise remarkably stable COCP dimer and to extract the carotenoid from this assembly. Moreover, this mechanism strongly suggests another novel biological role of COCP and its isolated homologs from other species, i.e., regarding proper chromophore integration and maturation of full-length OCP proteins.

#### Carotenoid shuttle mechanism between OCP domains—physiological implications

Our data demonstrate that the carotenoid, which is initially coordinated between two identical COCP monomers, undergoes spontaneous translocation, both, into the Apo-RCP module of OCP as well as the Apo-OCP module itself, resulting in formation of the orange OCP<sup>O</sup>-like state, which is then either photoconverted into RCP or results in reversibly photoswitchable OCP holoprotein. This as yet

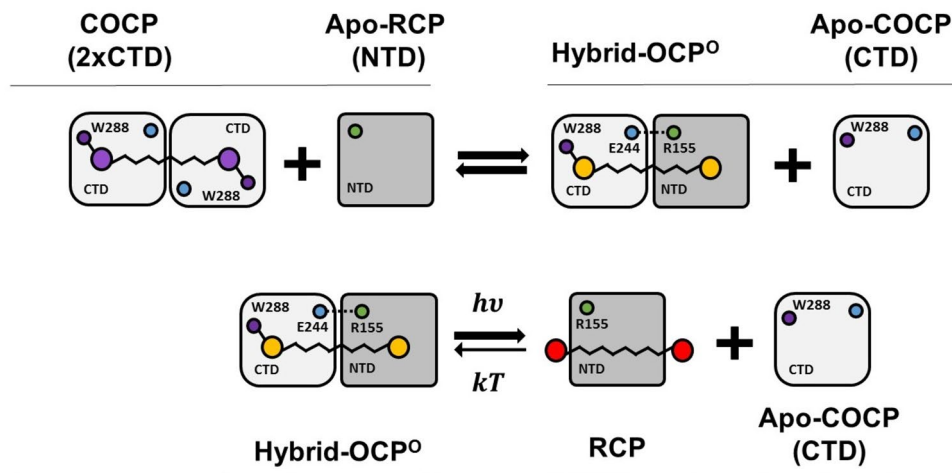


**Fig. 5** Schematic model of the interactions between COCP and Apo-RCP and the construction of a photoactive OCP orange-like heterodimer from these proteins. COCP acts like a carotenoid carrier. Since the NTD has higher affinity to the carotenoid than the CTD, Apo-RCP accepts the carotenoid from one of the two CTD subunits of

COCP, resulting in formation of a transient orange-like heterodimer (Hybrid OCP<sup>O</sup>). Upon photoactivation, the carotenoid may translocate completely into the NTD as the domain separation occurs (Gupta et al. 2015), ultimately causing release of an Apo-COCP module and the appearance of RCP

unprecedented carotenoid shuttle mechanism, which follows a scheme as outlined in Fig. 5, has profound physiological implications for the role of isolated OCP-CTD homologs in cyanobacteria. These physiological functions include the ability to maintain carotenoids in a soluble form for transport within or between cells, photoprotection by their profound ROS quenching activity, and carotenoid-shuttling devices that aid in chromophore integration of full-length OCP proteins, and, as demonstrated from the assembly of functional OCP from its CTD and NTD, being directly involved in cyanobacterial photoprotection by phycoobilisome fluorescence quenching.

Furthermore, our data unambiguously demonstrate that the OCP-CTD interacts tightly with FRP. Regarding the evolutionary history of OCP-mediated photoprotection in cyanobacteria, it seems likely that, having appeared independently in evolution, NTD and CTD precursors were combined at some point to form an ancestral protein similar to the currently known OCP, a notion that is supported by the observation that genes encoding isolated NTDs and CTDs are often encoded adjacent on the genome (Melnicki et al. 2016). The fact that isolated NTD and CTD homologs in cyanobacteria (sometimes combined with a full-length OCP homolog) still coexist indicates that, at least under some circumstances, the cell requires specialized functions of these protein modules independently from each other, which additionally supports their conservation as individual entities (Melnicki et al. 2016).

#### Assembly of OCP from domains—implications for protein engineering applications

The possibility to reconstruct a photoswitchable protein from its evolutionary units or domains immediately suggests a series of biotechnological applications. First, the extremely red-shifted absorption spectrum of COCP(CAN) underscores that there is considerable space for color-tuning of OCP-related proteins once a better understanding of the carotenoid–protein interactions is obtained that underlie the spectral properties, since, e.g., the most red-shifted carotenoid-binding protein, the astaxanthin-coordinating  $\beta$ -crustacyanine from the European lobster *Homarus gammarus* (Gamiz-Hernandez et al. 2015) has its maximum of the absorption spectrum at 590 nm. Second, the fact that COCP exclusively coordinates CAN upon expression in *E. coli* cells that produce mixtures of  $\beta$ -carotene, ECN and CAN opens the possibility to enrich certain carotenoids during biotechnological production in *E. coli*, which, based on protein engineering to alter carotenoid-binding preferences, could be expanded to facilitate production of pure preparations of even more complex xanthophylls. Third, the spontaneous assembly of COCP(CAN) with Apo-RCP opens a novel way to control biochemical processes

on demand by light, e.g., in the rapidly expanding field of optogenetics. Fusion of various output modules (or inactive fragments of such modules) to NTDs and CTDs of OCP-related proteins could be used to reconstruct functional activity on purpose and to trigger or terminate activity in a light-controlled fashion. The modular reconstruction of OCP from COCP(CAN) and Apo-RCP shown here rather results in the partly irreversible formation of RCP upon illumination, most likely due to the higher carotenoid-binding affinity of the RCP module. However, by modifying the carotenoid-binding properties of RCP (or by using some of the isolated CTD/NTD modules from other cyanobacterial genomes), the process could be engineered to become reversible to allow for multiple on-/off-switching cycles. It will be interesting to see whether such light-sensitive associating/disassembling modular systems based on OCP fragments already exist in nature, which might be disclosed once the multitude of isolated COCP and RCP homologs from cyanobacteria will be better characterized.

#### Significance for OCP-CTD homologs in cyanobacteria

Carotenoids abound in photosynthetic organisms and are essential nutrients for animals. Though they partition easily into lipid compartments or membranes due to their hydrophobic nature, only very few specific carotenoid-binding proteins are known, which have the potential to maintain carotenoids in a water-soluble form and to shuttle them between membranes or cells in the organism. These rare examples include the astaxanthin-binding crustacyanin from lobster carapace (Gamiz-Hernandez et al. 2015), the zeaxanthin-binding GSTP1 (Bhosale et al. 2004), the lutein-binding StARD3 from human retina (Li et al. 2011), and, besides OCP in cyanobacteria, the astaxanthin-binding AstaP (Kawasaki et al. 2013). Thus, identification of carotenoid-coordinating proteins, which can transport their cargo from the sites of biosynthesis to deliver it at places of need, is highly relevant for understanding the physiological implications of these molecules. This study adds another important carotenoid-binding entity, OCP-CTD and its hypothetical homologous proteins of as yet orphan function (Melnicki et al. 2016), to the molecular toolkit by which organisms might purposefully employ carotenoids. Many cyanobacteria have several separate genes for CTD and NTD homologs and combinatorial heteromeric assemblies of isolated NTDs and CTDs could substantially expand the variety of sensor/effecter modules based on OCP's architecture (López-Igual et al. 2016; Melnicki et al. 2016). These physiological roles may well include ROS quenching, general carotenoid transfer (e.g., from thylakoids to the outer membrane), or specific transfer to apoprotein forms of OCP and RCP homologs [or HCPs as proposed by (López-Igual et al. 2016)]. In particular, the

latter possibility could be a way to control the concentration of active quenchers of PBs fluorescence, and such a mechanism could be fully useful as a regulatory process for cyanobacteria. COCP belongs to the diverse superfamily of NTF-2-like proteins (PFAM 02136, nuclear transport factor 2-like) distributed in eu- as well as prokaryotes, which bind a variety of hydrophobic, frequently oxygenated substances. However, this family also includes enzymes like ketosteroid isomerase (Cho et al. 1998) or naphthalene 1,2-dioxygenase (Kauppi et al. 1998); thus, the functional spectrum of OCP-CTD homologs could even comprise catalysis. These possibilities exponentiate the molecular toolkit made up by carotenoid-binding proteins and opens a new field of research awaiting exploration.

**Acknowledgements** This work was supported by the German Ministry of Education and Research (WTZ-RUS Grant 01DJ15007 to M.M., N.N.T., F.-J.S. and T.F.), the German Research Foundation (Cluster of Excellence “Unifying Concepts in Catalysis” to T.F., D.B., and P.H.), the Russian Foundation for Basic Research (Grant 15-04-01930a to E.G.M.), the Russian Science Foundation (no. 14-17-00451 to E.G.M), and the Russian Ministry of Education and Science (Grant MK-5949.2015.4 to E.G.M.). E.G.M. was supported by Dynasty Foundation Fellowship. The study was funded by RFBR and Moscow City Government (research project № 15-34-70007 «mol\_a\_mos»). The authors thank Prof. N. Budisa and Dr. Tobias Baumann for providing access to CD spectroscopy equipment and Dr. M. Schlangen-Ahl for technical support during LC-MS experiments.

#### Compliance with ethical standards

**Conflict of interest** The authors declare that they have no conflict of interests.

## References

- Abraham MJ, Murtola T, Schulz R, Páll S, Smith JC, Hess B, Lindahl E (2015) GROMACS: High performance molecular simulations through multi-level parallelism from laptops to supercomputers. *SoftwareX* 1–2:19–25. doi:10.1016/j.softx.2015.06.001
- Bhosale P, Larson AJ, Frederick JM, Southwick K, Thulin CD, Bernstein PS (2004) Identification and characterization of a Pi isoform of glutathione S-transferase (GSTP1) as a zeaxanthin-binding protein in the macula of the human eye. *J Biol Chem* 279(47):49447–49454. doi:10.1074/jbc.M405334200
- Blankenship RE (2014) *Molecular Mechanism of Photosynthesis*. 2 edn. Wiley-Blackwell, Oxford, London, Edinburgh
- Boulay C, Wilson A, D’Haene S, Kirilovsky D (2010) Identification of a protein required for recovery of full antenna capacity in OCP-related photoprotective mechanism in cyanobacteria. *Proc Natl Acad Sci USA* 107(25):11620–11625. doi:10.1073/pnas.1002912107
- Britton G (1995) UV/Visible spectroscopy. In: Britton G, Liaaen-Jensen S, Pfander H (eds) *Carotenoids*, vol 1B. Birkhäuser, Basel
- Bryant DA (ed) (1994) *The molecular biology of cyanobacteria*, vol 1. Advances in photosynthesis and respiration. Springer, Dordrecht
- Chabera P, Durchan M, Shih PM, Kerfeld CA, Polivka T (2011) Excited-state properties of the 16 kDa red carotenoid protein from *Arthrospira maxima*. *Biochim Biophys Acta* 1807(1):30–35. doi:10.1016/j.bbabi.2010.08.013
- Cho H-S, Choi G, Choi KY, Oh B-H (1998) Crystal structure and enzyme mechanism of  $\Delta 5$ -3-ketosteroid isomerase from *Pseudomonas testosteroni*. *Biochemistry* 37(23):8325–8330. doi:10.1021/bi9801614
- Choi S-K, Nishida Y, Matsuda S, Adachi K, Kasai H, Peng X, Komemushi S, Miki W, Misawa N (2005) Characterization of  $\beta$ -carotene Ketolases, CrtW, from marine bacteria by complementation analysis in *Escherichia coli*. *Marine Biotechnol* 7(5):515–522. doi:10.1007/s10126-004-5100-z
- Cianci M, Rizkallah PJ, Olczak A, Raftery J, Chayen NE, Zagalsky PF, Helliwell JR (2002) The molecular basis of the coloration mechanism in lobster shell:  $\beta$ -Crustacyanin at 3.2-Å resolution. *Proc Natl Acad Sci USA* 99:9795–9800. doi:10.1073/pnas.152088999
- de Carbon CB, Thurotte A, Wilson A, Perreau F, Kirilovsky D (2015) Biosynthesis of soluble carotenoid holoproteins in *Escherichia coli*. *Sci Rep* 5:9085. doi:10.1038/srep09085
- Demmig-Adams B, Adams WW (1996) The role of xanthophyll cycle carotenoids in the protection of photosynthesis. *Trends Plant Sci* 1(1):21–26. doi:10.1016/S1360-1385(96)80019-7
- Demmig-Adams B, Garab G, Adams WW III, Govindjee (eds) (2014) Non-photochemical quenching and energy dissipation in plants, algae and cyanobacteria, vol 40. advances in photosynthesis and respiration. Springer, Dordrecht
- Gamiz-Hernandez AP, Angelova IN, Send R, Sundholm D, Kaila VRI (2015) Protein-induced color shift of carotenoids in  $\beta$ -Crustacyanin. *Angew Chem Intl Ed* 54(39):11564–11566. doi:10.1002/anie.201501609
- Govindjee, Shevela D (2011) Adventures with cyanobacteria: a personal perspective. *Front Plant Sci* 2(28):1–17. doi:10.3389/fpls.2011.00028
- Gupta S, Guttman M, Leverenz RL, Zhumadilova K, Pawlowski EG, Petzold CJ, Lee KK, Ralston CY, Kerfeld CA (2015) Local and global structural drivers for the photoactivation of the orange carotenoid protein. *Proc Natl Acad Sci USA* 112(41):E5567–E5574. doi:10.1073/pnas.1512240112
- Gwizdala M, Wilson A, Kirilovsky D (2011) *In vitro* reconstitution of the cyanobacterial photoprotective mechanism mediated by the orange carotenoid protein in *Synechocystis* PCC 6803. *Plant Cell* 23(7):2631–2643. doi:10.1105/tpc.111.086884
- Gwizdala M, Wilson A, Omairi-Nasser A, Kirilovsky D (2013) Characterization of the *Synechocystis* PCC 6803 fluorescence recovery protein involved in photoprotection. *Biochim Biophys Acta* 1827(3):348–354. doi:10.1016/j.bbabi.2012.11.001
- Kauppi B, Lee K, Carredano E, Parales RE, Gibson DT, Eklund H, Ramaswamy S (1998) Structure of an aromatic-ring-hydroxylating dioxygenase—naphthalene 1,2-dioxygenase. *Structure* 6(5):571–586. doi:10.1016/S0969-2126(98)00059-8
- Kawasaki S, Mizuguchi K, Sato M, Kono T, Shimizu H (2013) A novel astaxanthin-binding photooxidative stress-inducible aqueous carotenoprotein from a eukaryotic microalga isolated from asphalt in midsummer. *Plant Cell Physiol* 54(7):1027–1040. doi:10.1093/pcp/pct080
- Kerfeld CA, Sawaya MR, Brahmamdam V, Cascio D, Ho KK, Trevithick-Sutton CC, Krogmann DW, Yeates TO (2003) The crystal structure of a cyanobacterial water-soluble carotenoid binding protein. *Structure* 11(1):55–65. doi:10.1016/S0969-2126(02)00936-X
- King JD, Liu H, He G, Orf GS, Blankenship RE (2014) Chemical activation of the cyanobacterial orange carotenoid protein. *FEBS Lett* 588(24):4561–4565. doi:10.1016/j.febslet.2014.10.024
- Kirilovsky D, Kerfeld CA (2012) The orange carotenoid protein in photoprotection of photosystem II in cyanobacteria. *Biochim Biophys Acta* 1817(1):158–166. doi:10.1016/j.bbabi.2011.04.013

- Kish E, Pinto MM, Kirilovsky D, Spezia R, Robert B (2015) Echinonone vibrational properties: from solvents to the orange carotenoid protein. *Biochim Biophys Acta* 1847(10):1044–1054. doi:10.1016/j.bbabi.2015.05.010
- Leverenz RL, Jallet D, Li MD, Mathies RA, Kirilovsky D, Kerfeld CA (2014) Structural and functional modularity of the orange carotenoid protein: distinct roles for the N- and C-terminal domains in cyanobacterial photoprotection. *Plant Cell* 26(1):426–437. doi:10.1105/tpc.113.118588
- Leverenz RL, Sutter M, Wilson A, Gupta S, Thurotte A, Bourcier de Carbon C, Petzold CJ, Ralston C, Perreau F, Kirilovsky D, Kerfeld CA (2015) PHOTOSYNTHESIS. A 12 Å carotenoid translocation in a photoswitch associated with cyanobacterial photoprotection. *Science* 348(6242):1463–1466. doi:10.1126/science.aaa7234
- Li B, Vachali P, Frederick JM, Bernstein PS (2011) Identification of StARD3 as a lutein-binding protein in the macula of the primate retina. *Biochemistry* 50(13):2541–2549. doi:10.1021/bi101906y
- López-Igual R, Wilson A, Leverenz RL, Melnicki MR, Bourcier de Carbon C, Sutter M, Turmo A, Perreau F, Kerfeld CA, Kirilovsky D (2016) Different functions of the paralogs to the N-terminal domain of the orange carotenoid protein in the *Cyanobacterium Anabaena* sp. PCC 7120. *Plant Physiol* 171(3):1852–1866. doi:10.1104/pp.16.00502
- Luecke H, Schobert B, Stagno J, Imasheva ES, Wang JM, Balashov SP, Lanyi JK (2008) Crystallographic structure of xanthorhodopsin, the light-driven proton pump with a dual chromophore. *Proc Natl Acad Sci USA* 105(43):16561–16565. doi:10.1073/pnas.0807162105
- Maksimov EG, Schmitt FJ, Shirshin EA, Svirin MD, Elanskaya IV, Friedrich T, Fadeev VV, Paschenko VZ, Rubin AB (2014) The time course of non-photochemical quenching in phycobilisomes of *Synechocystis* sp. PCC6803 as revealed by picosecond time-resolved fluorimetry. *Biochim Biophys Acta* 1837(9):1540–1547. doi:10.1016/j.bbabi.2014.01.010
- Maksimov EG, Gvozdev DA, Strakhovskaya MG, Paschenko VZ (2015a) Hybrid structures of polycationic aluminum phthalocyanines and quantum dots. *Biochemistry (Moscow)* 80(3):323–331. doi:10.1134/S0006297915030074
- Maksimov EG, Klementiev KE, Shirshin EA, Tsoraev GV, Elanskaya IV, Paschenko VZ (2015b) Features of temporal behavior of fluorescence recovery in *Synechocystis* sp. PCC6803. *Photosynth Res* 125(1–2):167–178. doi:10.1007/s11120-015-0124-y
- Maksimov EG, Shirshin EA, Sluchanko NN, Zlenko DV, Parshina EY, Tsoraev GV, Klementiev KE, Budylin GS, Schmitt FJ, Friedrich T, Fadeev VV, Paschenko VZ, Rubin AB (2015c) The signaling state of orange carotenoid protein. *Biophys J* 109(3):595–607. doi:10.1016/j.bpj.2015.06.052
- Maksimov EG, Moldenhauer M, Shirshin EA, Parshina EA, Sluchanko NN, Klementiev KE, Tsoraev GV, Tavraz NN, Willoweit M, Schmitt FJ, Breitenbach J, Sandmann G, Paschenko VZ, Friedrich T, Rubin AB (2016) A comparative study of three signaling forms of the orange carotenoid protein. *Photosynth Res* 130(1–3):389–401. doi:10.1007/s11120-016-0272-8
- Maksimov EG, Sluchanko NN, Mironov KS, Shirshin EA, Klementiev KE, Tsoraev GV, Moldenhauer M, Friedrich T, Los DA, Allakhverdiev SI, Paschenko VZ, Rubin AB (2017) Fluorescent labeling preserving OCP photoactivity reveals its reorganization during the photocycle. *Biophys J* 112:46–56. doi:10.1016/j.bpj.2016.11.3193
- Mamedov M, Govindjee, Nadochenko V, Semenov A (2015) Primary electron transfer processes in photosynthetic reaction centers from oxygenic organisms. *Photosynth Res* 125(1):51–63. doi:10.1007/s11120-015-0088-y
- Melnicki MR, Leverenz RL, Sutter M, Lopez-Igual R, Wilson A, Pawlowski EG, Perreau F, Kirilovsky D, Kerfeld CA (2016) Structure, diversity, and evolution of a new family of soluble carotenoid-binding proteins in cyanobacteria. *Mol Plant* 9(10):1379–1394. doi:10.1016/j.molp.2016.06.009
- Mendes-Pinto MM, Sansiaume E, Hashimoto H, Pascal AA, Gall A, Robert B (2013) Electronic absorption and ground state structure of carotenoid molecules. *J Phys Chem B* 117(38):11015–11021. doi:10.1021/jp309908r
- Mirkovic T, Ostroumov EE, Anna JM, van Grondelle R, Govindjee, Scholes GD (2016) Light absorption and energy transfer in the antenna complexes of photosynthetic organisms. *Chem Rev* 117(2):249–293. doi:10.1021/acs.chemrev.6b00002
- Misawa N, Satomi Y, Kondo K, Yokoyama A, Kajiwara S, Saito T, Ohtani T, Miki W (1995) Structure and functional analysis of a marine bacterial carotenoid biosynthesis gene cluster and astaxanthin biosynthetic pathway proposed at the gene level. *J Bacteriol* 177(22):6575–6584. doi:10.1128/jb.177.22.6575-6584.1995
- Mori Y (2016) Computational study on the color change of 3'-hydroxyechinenone in the orange carotenoid protein. *Chem Phys Lett* 652:184–189. doi:10.1016/j.cplett.2016.04.062
- Niyogi KK, Truong TB (2013) Evolution of flexible non-photochemical quenching mechanisms that regulate light harvesting in oxygenic photosynthesis. *Curr Opin Plant Biol* 16(3):307–314. doi:10.1016/j.pbi.2013.03.011
- Schlücker S, Szeghalmi A, Schmitt M, Popp J, Kiefer W (2003) Density functional and vibrational spectroscopic analysis of  $\beta$ -carotene. *J Raman Spectr* 34(6):413–419. doi:10.1002/jrs.1013
- Schmitt F-J, Renger G, Friedrich T, Kreslavski VD, Zharmukhamedov SK, Los DA, Kuznetsov VV, Allakhverdiev SI (2014) Reactive oxygen species: re-evaluation of generation, monitoring and role in stress-signaling in phototrophic organisms. *Biochim Biophys Acta* 1837(6):835–848. doi:10.1016/j.bbabi.2014.02.005
- Sedoud A, Lopez-Igual R, Ur Rehman A, Wilson A, Perreau F, Boulay C, Vass I, Krieger-Liszkay A, Kirilovsky D (2014) The cyanobacterial photoactive orange carotenoid protein is an excellent singlet oxygen quencher. *Plant Cell* 26(4):1781–1791. doi:10.1105/tpc.114.123802
- Shevela D, Pishchalnikov RY, Eichacker LA, Govindjee (2013) Oxygenic photosynthesis in cyanobacteria. In: Srivastava AK, Rai AN, Neilan BA (eds) *Stress biology of cyanobacteria*. Taylor&Francis, Boca Raton, London, New York
- Sluchanko NN, Tugaeva KV, Faletrov YV, Levitsky DI (2016) High-yield soluble expression, purification and characterization of human steroidogenic acute regulatory protein (StAR) fused to a cleavable Maltose-Binding Protein (MBP). *Prot Expr Purif* 119:27–35. doi:10.1016/j.pep.2015.11.002
- Sluchanko NN, Klementiev KE, Shirshin EA, Tsoraev GV, Friedrich T, Maksimov EG (2017) The purple Trp288Ala mutant of *Synechocystis* OCP persistently quenches phycobilisome fluorescence and tightly interacts with FRP. *Biochim Biophys Acta* 1858:1–11. doi:10.1016/j.bbabi.2016.10.005
- Sutter M, Wilson A, Leverenz RL, Lopez-Igual R, Thurotte A, Salmeen AE, Kirilovsky D, Kerfeld CA (2013) Crystal structure of the FRP and identification of the active site for modulation of OCP-mediated photoprotection in cyanobacteria. *Proc Natl Acad Sci USA* 110(24):10022–10027. doi:10.1073/pnas.1303673110
- Thurotte A, López-Igual R, Wilson A, Comolet L, Bourcier de Carbon C, Xiao F, Kirilovsky D (2015) Regulation of orange carotenoid protein activity in cyanobacterial photoprotection. *Plant Physiol* 169(1):737–747. doi:10.1104/pp.15.00843
- Velazquez Escobar F, Hildebrandt T, Utesch T, Schmitt FJ, Seuffert I, Michael N, Schulz C, Mroginski MA, Friedrich T, Hildebrandt P (2013) Structural parameters controlling the fluorescence properties of phytochromes. *Biochemistry* 53(1):20–29. doi:10.1021/bi401287u
- Whitmore L, Wallace BA (2004) DICHROWEB, an online server for protein secondary structure analyses from circular

- dichroism spectroscopic data. *Nucleic Acid Res* 32 (Web Server issue):W668–W673. doi:[10.1093/nar/gkh371](https://doi.org/10.1093/nar/gkh371)
- Wilson A, Punginelli C, Gall A, Bonetti C, Alexandre M, Routaboul J-M, Kerfeld CA, van Grondelle R, Robert B, Kennis JTM, Kirilovsky D (2008) A photoactive carotenoid protein acting as light intensity sensor. *Proc Natl Acad Sci USA* 105(33):12075–12080. doi:[10.1073/pnas.0804636105](https://doi.org/10.1073/pnas.0804636105)
- Wilson A, Kinney JN, Zwart PH, Punginelli C, D'Haene S, Perreau F, Klein MG, Kirilovsky D, Kerfeld CA (2010) Structural determinants underlying photoprotection in the photoactive orange carotenoid protein of cyanobacteria. *J Biol Chem* 285(24):18364–18375. doi:[10.1074/jbc.M110.115709](https://doi.org/10.1074/jbc.M110.115709)

## Supplementary Information for

Assembly of photoactive Orange Carotenoid Protein from its domains unravels a carotenoid shuttle mechanism

Authors:

Marcus Moldenhauer, Nikolai N. Sluchanko, David Buhrke, Dmitry V. Zlenko, Neslihan N. Tavraz, Franz-Josef Schmitt, Peter Hildebrandt, Eugene G. Maksimov\* and Thomas Friedrich\*

correspondence to: [friedrich@chem.tu-berlin.de](mailto:friedrich@chem.tu-berlin.de), [emaksimoff@yandex.ru](mailto:emaksimoff@yandex.ru)

**This PDF file includes:**

Supplementary Text  
Supplementary Figures S1 to S6 including legends



## **Supplementary Text**

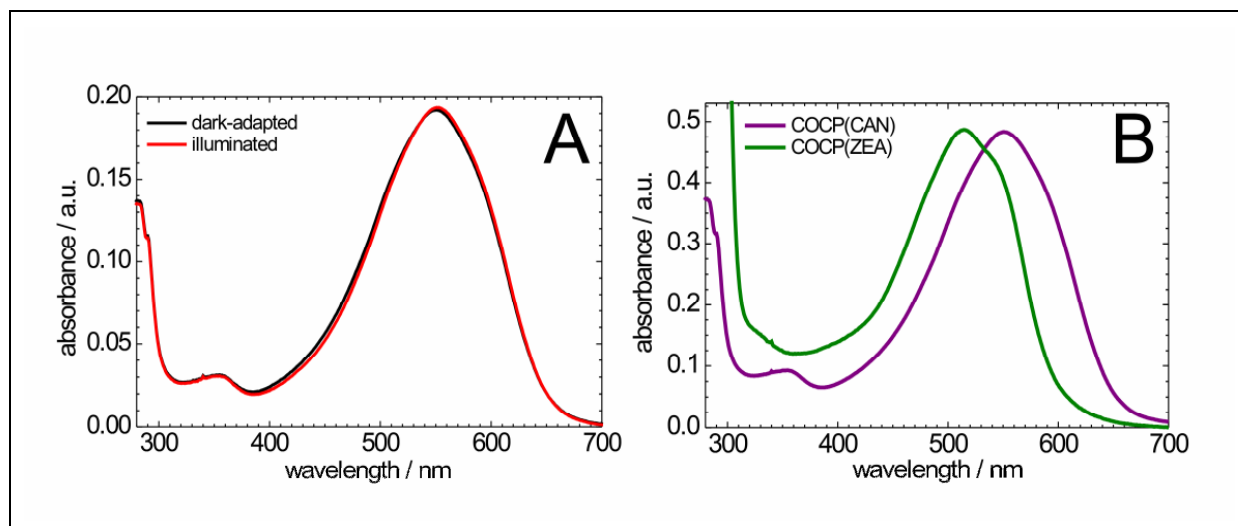
### **Carotenoid content of COCP and other OCP-related proteins**

Although the used *E. coli* strains expressed the CrtO ketolase from *Synechocystis*, which is actually considered a monoketolase (Fernández-González et al. 1997), and should accordingly produce mainly ECN, the carotenoid content of COCP and RCP was predominantly CAN (Supplementary Figure S4). Under the same cultivation conditions, the full-length OCP protein contained mostly ECN, suggesting different carotenoid preferences or conditions promoting symmetrical activity of the CrtO ketolase. COCP was also expressed in *E. coli* cells producing zeaxanthin (ZEA), again resulting in colored proteins with characteristic absorption spectra (Supplementary Figure S1B). These data suggest that COCP can accommodate carotenoids with symmetrical  $\beta$ -ring structures. Of note, expression of a mutant COCP protein carrying a substitution of the critical Trp residue involved in forming an H-bond to the 4-keto group of the xanthophyll (mutation Trp-288-Ala according to OCP amino acid numbering) in a CAN-producing *E. coli* strain yielded a CAN-coordinating protein (Supplementary Figure S1) with a less red-shifted absorption spectrum compared to the one of COCP (Figure 1D), which is only slightly red-shifted compared to the RCP absorption spectrum. This indicates that even the non-conservative W288A replacement does not abolish carotenoid binding to COCP and that the remaining H-bond to Tyr-201 might be sufficient for CAN binding. This also shows that distinct carotenoid-protein interactions pertaining to OCP must be intact in COCP, and that interference with the carotenoid coordination pattern affects color tuning. The spectral blue-shift upon W288A replacement in COCP is in stark contrast to the red-shifted absorption spectrum of the OCP-W288A mutant compared to OCP wildtype reported in previous work (Maksimov et al. 2016) indicating that the carotenoids experience strongly different environments in COCP, OCP and the corresponding W288A mutants.

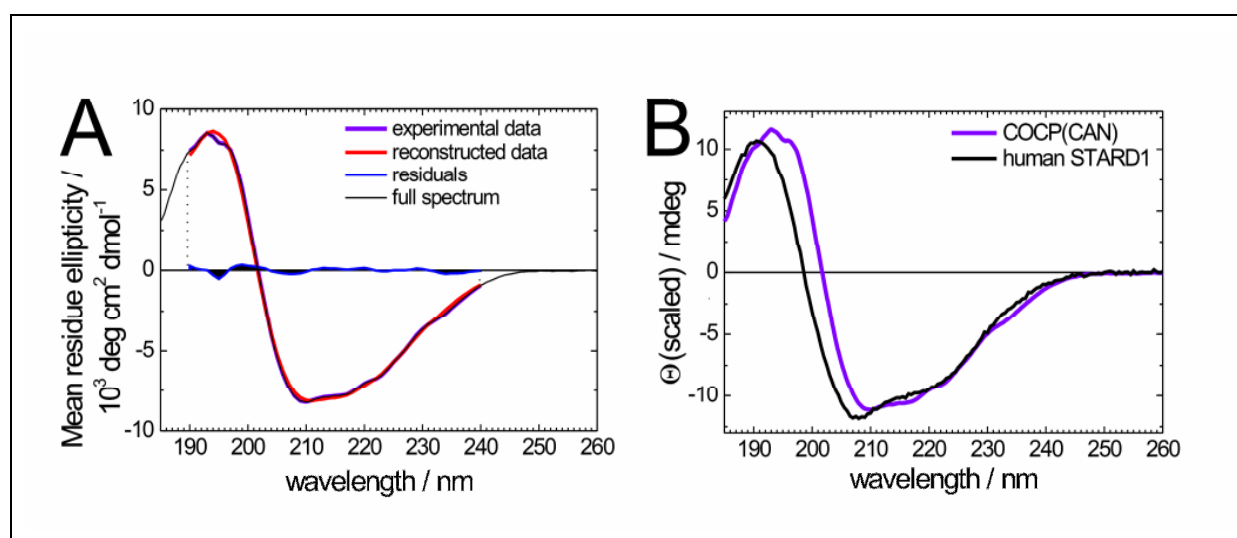
### **Functional activity of COCP, ROS quenching**

In order to access the  $^1\text{O}_2$  quenching capability in comparison to OCP, we produced  $^1\text{O}_2$  by illumination of either tetra- and pentakis(cholinile) aluminium phthalocyanines (AIPCs), which are characterized by high (up to 23%) yield of  $^1\text{O}_2$  production (Maksimov et al. 2015a) or by illuminating Rose Bengal, both in micromolar concentrations. Addition of carotenoid-containing proteins in micromolar concentration to the solution of AIPCs and singlet oxygen sensor green (SOSG, Life Technologies) caused a profound reduction of  $^1\text{O}_2$  yield. For

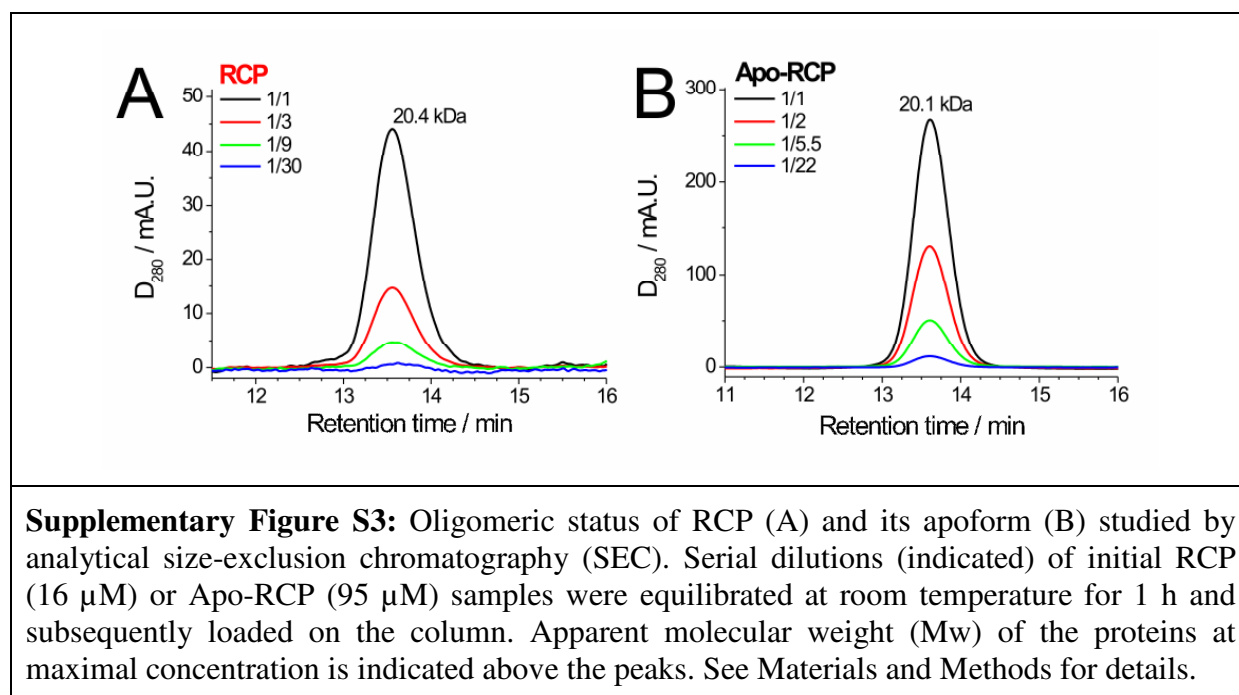
unknown reasons, we could not reach 50% reduction of  $^1\text{O}_2$  yield at 1.2-1.5  $\mu\text{M}$  concentrations by any of the carotenoid-containing proteins tested as it would be expected from previous studies (López-Igual et al. 2016; Sedoud et al. 2014), which is probably due to the differences in experimental conditions (photosensitizers, actinic light, ROS detection method, etc). However, since our experiments aiming at a comparison of  $^1\text{O}_2$  quenching of COCP and OCP were conducted under the same experimental conditions, the results are relevant. Surprisingly, COCP appears to be even a better  $^1\text{O}_2$  quencher than OCP in the orange state. Similar tests with Rose Bengal as  $^1\text{O}_2$  sensitizer, as used in previous assays on  $^1\text{O}_2$  quenching by OCP proteins (Kerfeld et al. 2003; Sedoud et al. 2014) also showed  $^1\text{O}_2$  quenching activity of COCP outperforms the one of OCP<sup>O</sup>. This feature of COCP could be related to its functional role *in vivo*.

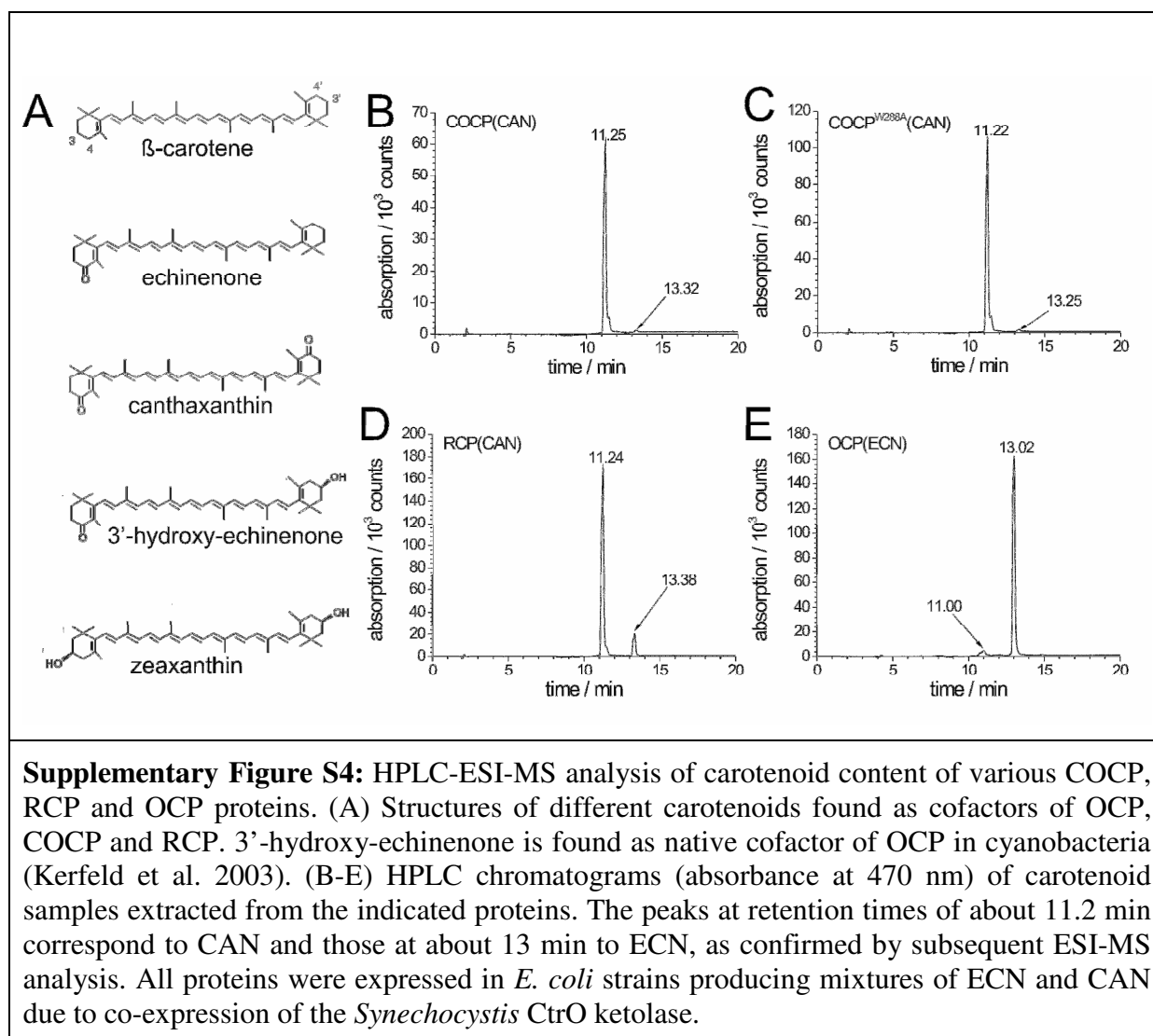


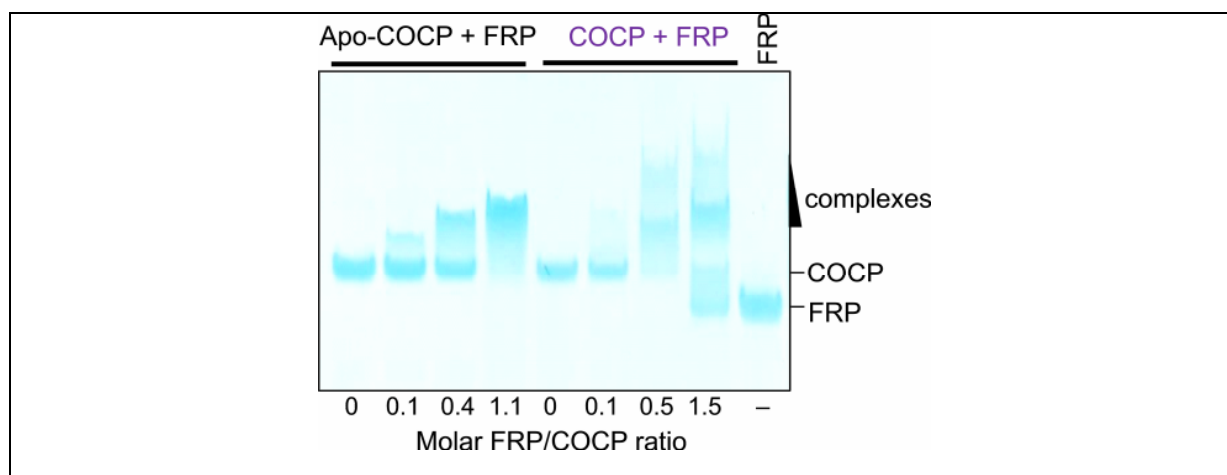
**Supplementary Figure S1:** (A) Absorption spectra of COCP before (dark-adapted) and after 5 min illumination with actinic light (455 nm LED, 900 mW) and (B) of COCP proteins obtained upon expression in *E. coli* strains producing canthaxanthin (CAN), as in (A), or zeaxanthin (ZEA).



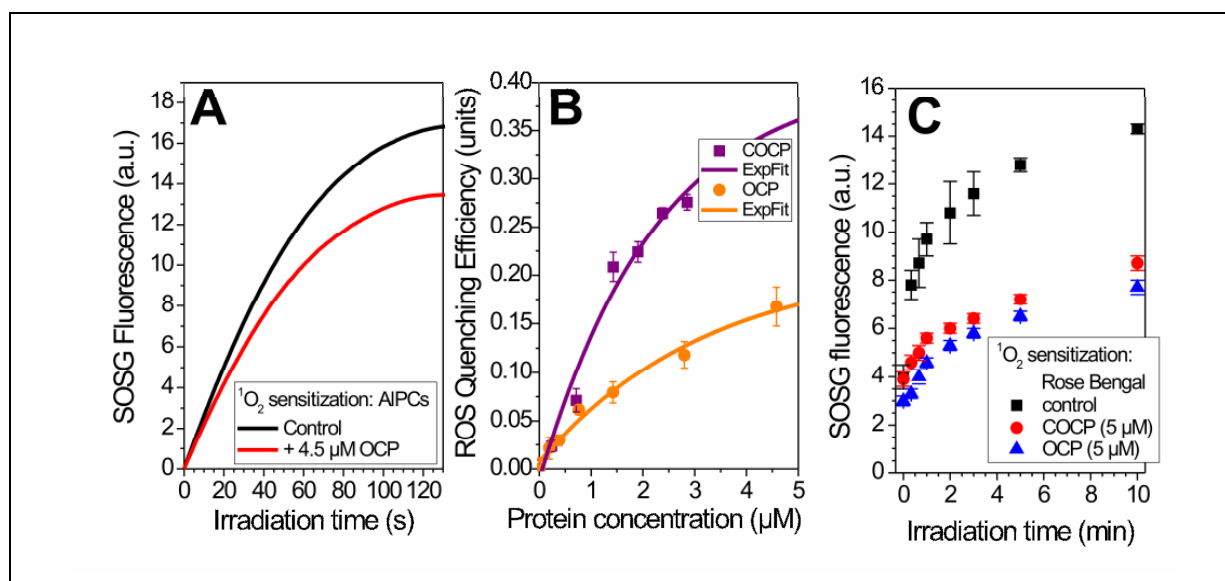
**Supplementary Figure S2:** Far UV-CD spectrum of COCP and analysis of its secondary structure by deconvolution using the CDSSTR algorithm available on the DichroWeb server (Whitmore and Wallace 2004). (A) COCP (0.15 mg/ml or 8.3  $\mu\text{M}$  per monomer) was measured in 30 mM sodium phosphate buffer, pH 7.4, at 20 °C on a J-1100 CD spectrometer (Jasco) using a 1 mm cell. For deconvolution, the range 190-240 nm and the protein dataset 4 of DichroWeb were taken. The best fitting algorithm, CDSSTR, produced the fit with the lowest NRMSD value (0.027), yielding 15 %  $\alpha$ -helices, 32 %  $\beta$ -strands, and 53 % irregular structures. (B) Similarity of the fold of Apo-COCP (violet) (PDB 4xb5 for OCP, residues 165-314) and that of an unrelated cholesterol-binding human steroidogenic acute regulatory protein domain (STARD1) (PDB 3POL chain A, residues 64-276) having 19 %  $\alpha$ -helices, 31 %  $\beta$ -strands, and 50% irregular structures (Sluchanko et al. 2016). The slightly larger proportion of  $\alpha$ -helices in STARD1 is reflected by the more pronounced minima at 208 and 222 nm.





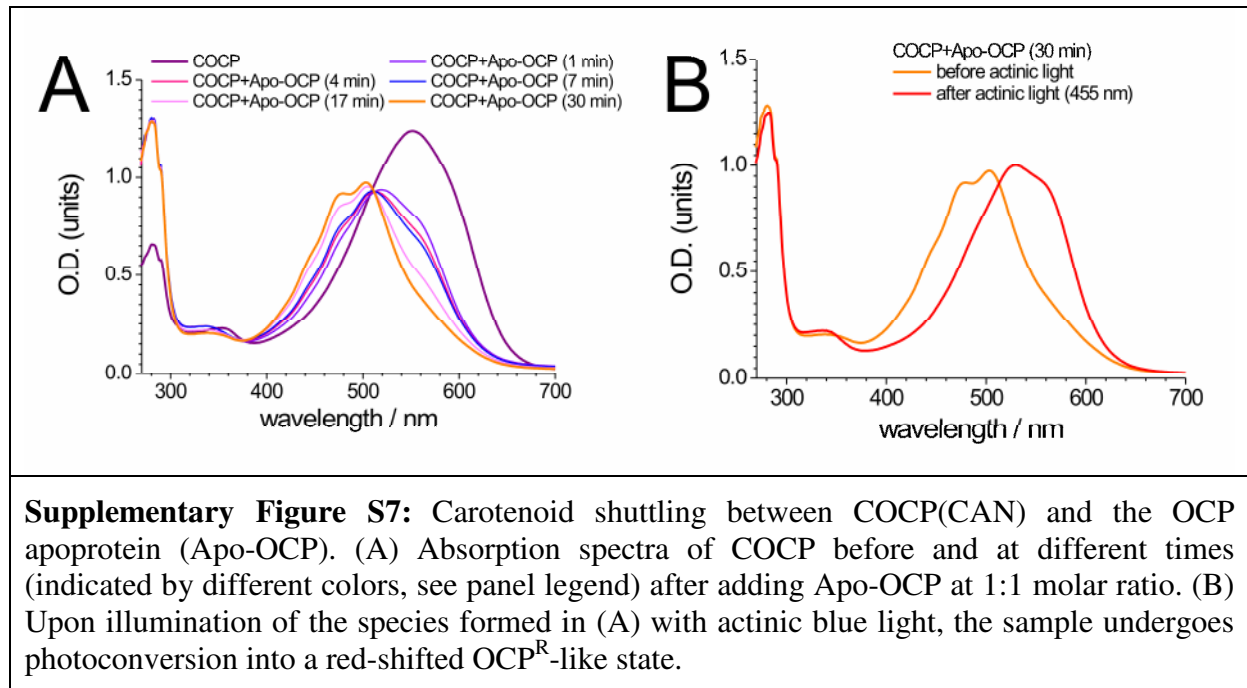


**Supplementary Figure S5:** Interaction of COCP and Apo-COCP with FRP analyzed by native-PAGE stained by Coomassie brilliant blue. Apo-COCP (90  $\mu\text{M}$ ) or COCP(CAN) (60  $\mu\text{M}$ ) were pre-incubated in the presence of increasing FRP concentrations (at molar ratios as indicated below the gel) and then subjected to electrophoresis at pH 8.6. FRP alone was loaded on the last lane, and the positions of the species are indicated on the right. Note, that excision of the complex band followed by SDS-PAGE validated the presence of both proteins (data not shown). The presence of carotenoids in COCP does not affect their ability to interact with FRP, however, the stoichiometry of COCP/FRP interaction may vary.



**Supplementary Figure S6:**  $^1\text{O}_2$  quenching activity of COCP and OCP. (A) Time-course of  $^1\text{O}_2$  accumulation (detected by fluorescence of 2  $\mu\text{M}$  Singlet Oxygen Sensor Green, SOSG) in the absence and in presence of OCP. A mixture of AIPCs (4  $\mu\text{M}$ ) was added to 1 ml of buffer. Light from a 625 nm LED (230 mW), filtered through a 600 nm long-pass filter (to prevent photoactivation of OCP), was used for the photosensitized generation of  $^1\text{O}_2$  from AIPCs at 25  $^\circ\text{C}$  under constant stirring. (B) Efficiency of  $^1\text{O}_2$  quenching by OCP (orange form) and COCP (violet). Quenching efficiency was calculated as a reduction of maximal SOSG intensity reached upon illumination of the sample. (C) Time-course of  $^1\text{O}_2$  accumulation (detected by 1  $\mu\text{M}$  SOSG fluorescence) using 1  $\mu\text{M}$  Rose Bengal in the absence (blue) and in presence of OCP (black) or COCP (red). The solution was illuminated by red light from a halogen lamp (2000  $\text{W}/\text{cm}^2$ , 570 nm long-pass filter) at 22  $^\circ\text{C}$ .





**Supplementary Figure S7:** Carotenoid shuttling between COCP(CAN) and the OCP apoprotein (Apo-OCP). (A) Absorption spectra of COCP before and at different times (indicated by different colors, see panel legend) after adding Apo-OCP at 1:1 molar ratio. (B) Upon illumination of the species formed in (A) with actinic blue light, the sample undergoes photoconversion into a red-shifted OCP<sup>R</sup>-like state.